crystals

MDPI

Review

Perplexing Coordination Behaviour of Potentially Bridging Bipyridyl-Type Ligands in the Coordination Chemistry of Zinc and Cadmium 1,1-Dithiolate Compounds

Edward R. T. Tiekink

Research Centre for Crystalline Materials, School of Science and Technology, Sunway University, No. 5 Jalan Universiti, Bandar Sunway 47500, Selangor Darul Ehsan, Malaysia; edwardt@sunway.edu.my; Tel.: +60-3-7491-7181

Received: 9 December 2017; Accepted: 31 December 2017; Published: 4 January 2018

Abstract: The X-ray structural chemistry of zinc and cadmium 1,1-dithiolates (for example, xanthate, dithiophosphate and dithiocarbamate) with potentially bridging bipyridyl-type ligands (for example, 4,4′-bipyridine) is reviewed. For zinc, the xanthates and dithiophosphates uniformly form one-dimensional coordination polymers, whereas the zinc dithiocarbamates are always zero-dimensional, reflecting the exceptional chelating ability of dithiocarbamate ligands compared with xanthates and dithiophosphates. For cadmium, one-dimensional coordination polymers are usually found, reflecting the larger size of cadmium compared with zinc, but zero-dimensional aggregates are sometimes found. Steric effects associated with the 1,1-dithiolate-bound R groups are shown to influence supramolecular aggregation and, when formed, polymer topology in order to reduce steric hindrance; the nature of the bipyridyl-type ligand can also be influential. For the dithiocarbamates of both zinc and cadmium, in instances where the dithiocarbamate ligand is functionalised with hydrogen bonding potential, extended supramolecular architectures are often formed via hydrogen bonding interactions. Of particular interest is the observation that the bipyridyl-type ligands do not always bridge zinc or cadmium 1,1-dithiolates, being monodentate instead, often in the presence of hydrogen bonding. Thus, hydroxyl-O–H $\cdots$ N(pyridyl) hydrogen bonds are sometimes formed in preference to M←N(pyridyl) coordinate-bonds, suggesting a competition between the two modes of association.

Keywords: crystal engineering; coordination polymers; hydrogen bonding; structural chemistry; zinc; cadmium; dithiocarbamate; xanthate; dithiophosphates; unusual coordination modes

1. Introduction

Bioinorganic chemistry, incorporating investigations into the natural functions of metals in biology to the development of metal-based therapeutics and diagnostic agents, has been the mainstay of coordination chemistry, involving transitions metals, main group elements and lanthanides, for many decades. However, this dominance is increasingly challenged by the development of coordination polymers of various dimensions up to and including three-dimensions, that is, metal-organic framework structures. This interest is reflected in the now over 70,000 X-ray crystal structures of coordination polymers [1] included in the Cambridge Structural Database [2]. A myriad of potential applications prompt investigations into coordination polymers. While these were initially in the realm of materials science with applications relating to energy and gas storage, photo-responsive materials, catalysis, etc. [3–7], there are increasing applications of coordination polymers relevant to bioinorganic chemists. Examples include coordination polymers functioning as carriers for drug

delivery, biosensors and as therapeutics themselves [8–11]. Coordination polymers are now being constructed from biologically relevant materials [12,13].

Coordination polymers are typically neutral and are constructed from a combination of charged and neutral ligands; it is noted that charged coordination polymers are also known. Increasing the functionality of the ligands enhances the probability of attaining the three-dimensional metal–organic frameworks. Charged ligands for complexation are exemplified by carboxylates derived from, for example, acetic acid, terephthalic acid (benzene-1,4-dicarboxylic acid) and trimesic acid (benzene-1,3,5-tricarboxylic acid); that is, a series with increasing bridging capacity. In the same way, potentially bridging bipyridyl-type ligands are prominent in building coordination polymers with the most prominent example being 4,4′-bipyridine. The combination of these and related building blocks have been extensively exploited by the research groups of, for example, Fujita [14,15], Yaghi [16,17] and Zaworotko [18,19].

A class of ligands closely related to carboxylate ligands is the 1,1-dithiolates, having two sulphur atoms connected to the quaternary carbon atom rather than two oxygens. Prominent examples of 1,1-dithiolate ligands include xanthates, dithiophosphates and dithiocarbamates, Figure 1. Despite the chemical similarity of the 1,1-dithiolates with carboxylate, the evaluation of the propensity of these ligands to form coordination polymers is generally lacking. This is perhaps a little surprising given that 1,1-dithiolate ligands are well known to form bridges between metal centres [20–24], especially in the binary 1,1-dithiolates of the zinc-triad elements [25]. Indeed, it was the desire to destroy this supramolecular aggregation by the addition of nitrogen-bases that was the original motivation for investigating this chemistry, as the resulting smaller aggregates were found to be more useful as synthetic precursors for chemical vapour deposition of metal sulphide nanomaterials.

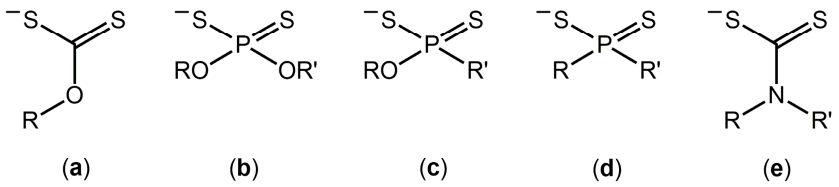

Figure 1. Chemical diagrams for (**a**) xanthate (*O*-alkyldithiocarbonate); (**b**) dithiophosphate; (**c**) dithiophosphonate; (**d**) dithiophosphinate; and (**e**) dithiocarbamate. R, R′ = alkyl, aryl.

In this bibliographic review, the structural chemistry of zinc and cadmium 1,1-dithiolates and bipyridyl-type ligands is surveyed. While one-dimensional coordination polymers are observed, there are no examples of two- let alone three-dimensional coordination polymers, at least not stabilised by bonds involving zinc or cadmium, that is, by a combination of covalent and coordinate-bonding interactions. Despite this, an interesting structural chemistry is frequently revealed. For example, often in the presence of hydrogen bonding functionality in the 1,1-dithiolate ligands, putative coordinate-bonding between zinc or cadmium and the bipyridyl-type ligand is suppressed to allow for the formation of competing hydrogen bonding interactions.

2. Methodology and Organisation

The structures included in this survey were extracted in the form of crystallographic information files (CIFs) from the Cambridge Structural Database (CSD, 2017 release with updates) [2]. Data were analysed using PLATON [26] and diagrams drawn with the graphics program DIAMOND [27]. The review is divided into a discussion of zinc structures followed by those of cadmium. Within in each category, xanthate species are discussed before dithiophosphates (and lesser known derivatives) and then dithiocarbamates. A diverse variety of bipyridyl-type ligands are represented among the structures and their chemical diagrams with abbreviations are shown in Figure 2. As a general principal, smaller bipyridyl-type ligands are discussed before larger/more complicated analogues

and for each type of bipyridyl-type ligand, the molecules/aggregates are described in terms of the bulk of the R/R′ substituents of the 1,1-dithiolate ligand, with smaller groups discussed first. The discussion is focussed upon a general description of the modes of coordination of the 1,1-dithiolate and bipyridyl-type ligands and describing the resultant aggregation patterns. Details of geometric parameters are available in the original publication and are not generally considered. Similarly, generally descriptions of molecular packing are avoided unless relevant to the putative competition between hydrogen bonding and M←N(pyridyl) coordinate-bonds. In all, there are 57 zinc-containing structures and 31 cadmium analogues.

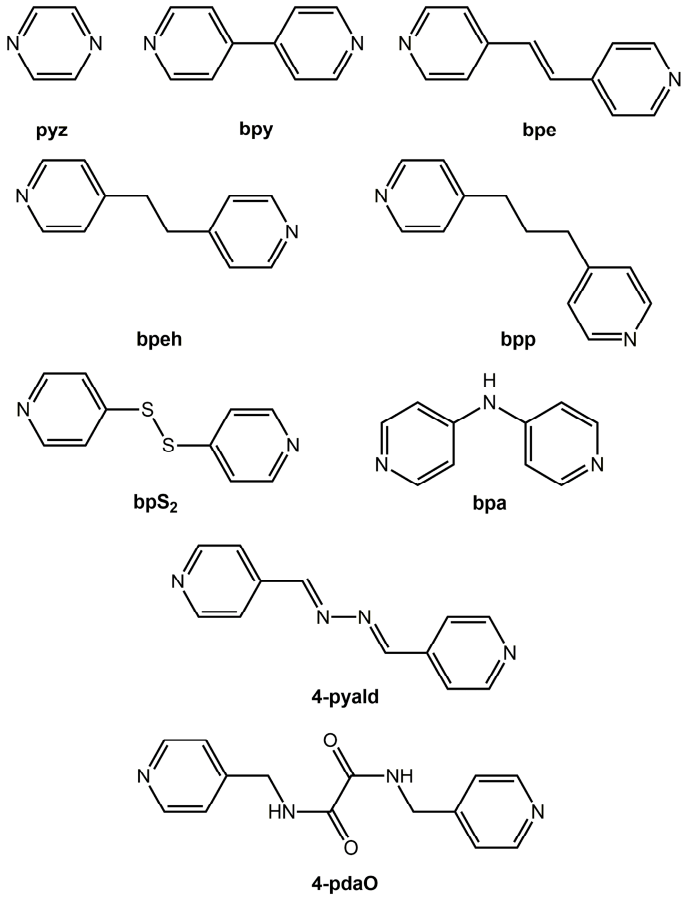

Figure 2. Chemical diagrams for bipyridyl-type ligands discussed in this review and their abbreviations: (**pyz**) pyrazine, (**bpy**) 4,4′-bipyridine, (**bpe**) *trans*-1,2-bis(4-pyridyl)ethylene, (**bpeh**) *trans*-1,2-bis(4-pyridyl)ethane, (**bpp**) *trans*-1,2-bis(4-pyridyl)propane, (**bpS$_2$**) bis(4-pyridyl)disulphide, (**bpa**) bis(4-pyridyl)amine, (**4-pyald**) 1,2-bis(4-pyridylmethylene)hydrazine and (**4-pdaO**) N,N′-bis (pyridin-4-ylmethyl)ethanediamide. Abbreviations for isomers and derivatives of the above: **2-bpe**, 2-pyridyl isomer of bpe; **3-pyald** and **2-pyald**, 3- and 2-pyridyl isomers of 4-pyald; **3-pdaO**, 3-pyridyl isomer of 4-pdaO; **3-pdaOt**, hydroxyl-imine tautomer of 3-pdaO; **3-pdaS**, thio analogue of 3-pdaO.

3. Discussion

3.1. Zinc Xanthate Structures

There are six structures in this category, **1**–**6** [28–31], and general features of these are summarised in Table 1 along with the other zinc structures, **1**–**57** [28–66], included in this survey. The first structure to be described contains the smallest bipyridyl-type ligand, namely pyrazine (pyr), and is a one-dimensional coordination polymer formulated as $[Zn(S_2COEt)_2(pyr)]_n$ (**1**) [28]. In **1**, Figure 1a, the zinc atom lies on a special position 2/m and the pyr ligand lies about a two-fold axis with the

nitrogen atoms lying on the axis. The xanthate ligands are S,S-chelating and the resulting *trans*-N_2S_4 donor set defines a distorted octahedral geometry. The topology of the chain is strictly linear owing to the aforementioned symmetry. It is apposite here to comment on the structure of the parent molecule found in **1**; that is, $[Zn(S_2COEt)_2]_n$ [67,68]. Here, each xanthate ligand is bidentate bridging and the resulting two-dimensional structure is conveniently described as being constructed by an infinite pattern of edge-shared squares, with each square comprising zinc atoms and with pairs of adjacent zinc atoms being bridged by a xanthate ligand resulting in ZnS_4 tetrahedra. With the addition of base, pillaring of the layers into a three-dimensional architecture might be envisaged, with suitable adjustments in the coordination geometries about the zinc atoms. Instead, the original two-dimensional architecture of $[Zn(S_2COEt)_2]_n$ is disrupted in **1** to form a one-dimensional aggregation pattern. This principle of perturbing the supramolecular architecture observed in the parent 1,1-dithiolate structure is generally applicable to the structures described herein.

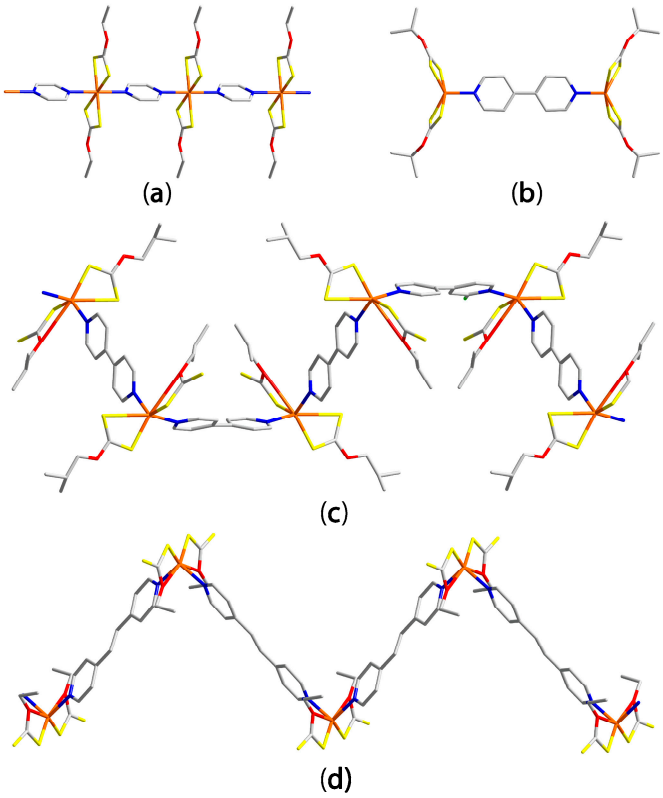

Figure 3. Aggregation in the structures of (**a**) $[Zn(S_2COEt)_2(pyr)]_n$ (**1**); (**b**) $[Zn(S_2COiPr)_2]_2(bpy)$ (**2**); (**c**) $[Zn(S_2COiBu)_2(bpy)]_n$ (**3**); and (**d**) $[Zn(S_2COEt)_2(bpe)]_n$ (**4**). Colour code: zinc or cadmium, orange; sulphur, yellow; oxygen, red, nitrogen, blue; carbon, grey. Non-acidic hydrogen atoms and non-participating species, typically solvent molecules, have been omitted in all diagrams.

Table 1. Summary of the general features of zinc structures **1**–**57** [28–66].

Compound	R/R′	N-Ligand	Donor Set	Motif	Ref.
1	Et	pyr	N_2S_4	linear chain	[28]
2 [1]	iPr	bpy	NS_4	dimer	[29]
3	iBu	bpy	N_2OS_3	helical chain	[30]
4	Et	bpe	$N_2O_2S_2$	zig-zag chain	[31]
5	nBu	bpe	$N_2O_2S_2$	zig-zag chain	[31]
6 [2]	Cy	bpe	NS_4	dimer	[31]
7	iPr	pyr	NS_3+S	dimer	[32]

Table 1. *Cont.*

Compound	R/R′	N-Ligand	Donor Set	Motif	Ref.
8	Et	bpy	N_2S_2 N_2OS_2	zig-zag chain	[33]
9	iPr	bpy	N_2S_2	zig-zag chain	[34]
10	Cy	bpy	NS_4	dimer	[35]
11	iPr	bpe	N_2S_2	zig-zag chain	[36]
12	iBu	bpe	N_2S_4	linear chain	[37]
13	Cy	bpe	N_2S_4	linear chain	[35]
14 [3]	iPr	bpeh	NS_4	dimer	[38]
15	Et	bpeh	N_2S_2	zig-zag chain	[35]
16 [4]	iPr	bpeh	N_2S_2	zig-zag chain	[35]
17	iBu	bpeh	N_2S_4	linear chain	[39]
18	Cy	bpeh	N_2S_2	zig-zag chain	[35]
19	iPr	bpp	N_2S_2	helical chain	[32]
20	iPr	bpS_2	N_2OS_2	zig-zag chain	[32]
21	iPr	bpa	N_2S_2	zig-zag chain	[32]
22	Cy	4-pyald	N_2S_4	zig-zag chain	[40]
23	iPr	2-bpe	NS_4	dimer	[32]
24	Cy	2-bpe	NS_3	monomer	[32]
25	iPr	3-pyald	N_2S_4	linear chain	[41]
26	Me, 4-MePh	bpeh	N_2S_2	zig-zag chain	[42]
27	iBu	bpy	N_2S_4	linear	[43]
28	nPr	bpy	NS_4	monomer	[44]
29	Me	bpy	NS_4	dimer	[45]
30	Et	bpy	NS_4	dimer	[49,50]
31	nPr	bpy	NS_4	dimer	[44]
32 [5]	iPr	bpy	NS_4	dimer	[48]
33	iBu	bpy	NS_4	dimer	[49]
34	CH_2Ph	bpy	NS_4	dimer	[50]
35 [6]	CH_2CH_2	bpy	NS_4	dimer	[51]
36 [7]	CH_2CH_2	bpy	NS_4	dimer	[52]
37	Me	bpe	NS_4	dimer	[53]
38 [8]	Et	bpe	NS_4	dimer	[54]
39	iPr	bpe	NS_4	dimer	[55]
40 [9]	Et	bpe	NS_4	dimer	[56]
41	nPr	bpeh	NS_4	dimer	[57]
42	Et	4-pdaO	NS_4	dimer	[58]
43 [10]	Me	3-pdaO	NS_4	dimer	[59]
44	nPr	3-pdaO	NS_4	dimer	[59]
45	CH_2CH_2OH	pyr	NS_4	dimer	[60]
46 [11]	CH_2CH_2OH	pyr	NS_4	dimer	[60]
47	Me, CH_2CH_2OH	bpy	NS_4	dimer	[61]
48	Et, CH_2CH_2OH,	bpy	NS_4	dimer	[61]
49 [12]	Et, CH_2CH_2OH	bpy	NS_4	dimer	[61]
50	CH_2CH_2OH	bpy	NS_4	dimer	[61]
51 [13]	iPr, CH_2CH_2OH	bpy	NS_4	monomer	[62]
52	Me, CH_2CH_2OH	4-pyald	NS_4	monomer	[63]
53	Me, CH_2CH_2OH	3-pdaO	NS_4	dimer	[64]
54	CH_2CH_2OH	3-pdaOt	NS_4	dimer	[64]
55 [10]	Me, CH_2CH_2OH	3-pdaS	NS_4	dimer	[65]
56 [14]	Me, CH_2CH_2OH	3-pdaS	NS_4	dimer	[65]
57 [15]	Me, CH_2CH_2OH	triazine	N_3S_2	monomer	[66]

[1] Dichloromethane mono-solvate; [2] Chloroform di-solvate; [3] Acetonitrile di-solvate; [4] Chloroform hemi-solvate; [5] Toluene di-solvate; [6] NR_2 = pyrrolidine; [7] NR_2 = piperidine; [8] Chloroform mono-solvate; [9] Co-crystallised with one uncoordinated bpe molecule; [10] Dimethylformamide di-solvate; [11] Dioxane di-solvate; [12] Methanol di-solvate; [13] Co-crystallised with half an uncoordinated bpy molecule; [14] Co-crystallised with two S_8 molecules molecule; [15] Dioxane sesqui-solvate.

The next structures to be described feature the 4,4′-bipyridine (bpy) ligand which is well represented in the present survey. The structure of $[Zn(S_2COiPr)_2]_2(bpy)$ (**2**) [29] is shown in Figure 1b and is binuclear; the molecule has two-fold symmetry with the zinc atoms lying on the axis. The xanthate ligands are S,S-chelating and the five-coordinate geometries are completed by a pyridyl-N atom. The NS_4 donor set is heavily distorted with the value of τ computing to 0.63, which compares to 1.0 for an ideal trigonal-bipyramid and 0.0 for an ideal square-pyramid [69]. The second zinc xanthate structure with bpy is a coordination polymer as the ratio of components is 1:1 rather than 2:1 as in **2**. In $[Zn(S_2COiBu)_2(bpy)]_n$ (**3**) [30], one xanthate ligand is S,S-chelating but with disparate Zn–S bond lengths while the other is S,O-chelating with the Zn-O separation being long at 3.11 Å. While comparatively rare, such S,O-chelating modes are known in the structural chemistry of metal xanthates [20]. In **3**, the resulting N_2OS_3 coordination geometry is based on a distorted octahedron. The topology of the chain is helical, Figure 1c. A difference in the conformation of the bpy ligand in the structures of **2** and **3** is noted, namely the dihedral angle between the pyridyl rings in **2** is 13.9° compared with 29.0° in **3**, indicating conformational flexibility. The three remaining structures in this section contain the *trans*-1,2-bis(4-pyridyl)ethylene (bpe) ligand in a bridging mode [31]. In $[Zn(S_2COR)_2(bpe)]_n$, for R = Et (**4**) and nBu (**5**), both xanthate ligands are S,O-chelating resulting in $N_2O_2S_2$ donor sets which are best described as being skew-trapezoidal bipyramidal in which the pyridyl-N atoms lie over the relatively long Zn–O bonds. The coordination polymer in each of **4** and **5** has a zig-zag topology as illustrated for **4** in Figure 1d. When the steric bulk of the R group in the xanthate ligand is increased, a new aggregation pattern in observed. In $[Zn(S_2COCy)_2]_2(bpe)$ (**6**) [31], isolated from analogous 1:1 solutions that yielded **4** and **5**, the xanthate ligands revert to S,S-coordination modes and a binuclear aggregate is formed, similar to that shown in Figure 1b. Such steric effects in the coordination chemistry of metal 1,1-thiolates is well documented [25,68,70]. With τ = 0.51, the NS_4 coordination geometry in **6** is almost exactly intermediate between the two ideal five-coordinate geometries. The influence of aggregation patterns in **4**–**6**—that is, polymeric versus dimeric—was shown to have a distinct influence upon the solid-state luminescence responses [31].

Although only including six structures, the foregoing offers a microcosm of the variability of structures covered in this review. Thus, different coordination modes of the xanthate ligand are evident leading to distinct coordination geometries, different aggregation patterns, sometimes related to the steric bulk of the substituents, and, when formed variable topologies of coordination polymers and conformational variations in the bridging ligands.

3.2. Zinc Dithiophosphate and Related Structures

The first dithiophosphate structure to be described in this section is a centrosymmetric binuclear species similar to that observed for **2**, Figure 1b. In $\{Zn[S_2P(OiPr)_2]_2\}_2(pyr)$ (**7**) [32], one dithiophosphate ligand is chelating while the other, with Zn–S bond lengths differing by nearly 1 Å, is coordinating in an asymmetric mode or taken to an extreme, is monodentate. The NS_3 donor set is distorted tetrahedral with the widest angle at the zinc atom of approximately 132° correlating with the close approach of the non-coordinating sulphur atom. Crystals of **7** were isolated from solutions containing a 1:1 ratio of reagents but only the 2:1 species was isolated [32]. As evident from Figure 4a, the environment about the binuclear is congested and steric hindrance is likely the cause for the lack of polymer formation.

Compounds **8**–**10** involve bridging bpy ligands. In $\{Zn[S_2P(OEt)_2]_2(bpy)\}_n$ (**8**) [33], two independent formula units comprise the asymmetric unit. One of the independent zinc atoms is coordinated within a distorted tetrahedral N_2S_2 donor set; both dithiophosphate ligands coordinate in the monodentate mode. By contrast, the second independent zinc atom is five coordinate as one of the dithiophosphate ligands is S,O-coordinating. The NO_2S_2 donor set is intermediate between ideal trigonal-bipyramidal and square-pyramidal geometries (τ = 0.53). There are three independent bpy molecules in the structure with two located about a centre of inversion. For these, the twist between rings is 0°. For the bpy molecule bridging the independent zinc atoms, the twist is 29°. The resultant coordination polymer has a zig-zag topology as shown in Figure 4b. To a first approximation, a similar coordination polymer

is found in the crystal of $\{Zn[S_2P(OiPr)_2]_2(bpy)\}_n$ (**9**) [34]. The asymmetric unit of **9** comprises four independent repeat units but, each zinc atom exists within a distorted tetrahedral N_2S_2 donor set. The dihedral angles for the bpy ligands range from 26 to 45°. The third structure has bulky cyclohexyl substituents and therefore, owing to steric hindrance, only binuclear $\{Zn[S_2P(OCy_2)_2]_2\}_2(bpy)$ (**10**) [35] could be isolated. Here, the dithiophosphate ligands coordinate in a S,S-mode leading to a NS_4 donor set which tends towards a square-pyramidal geometry with the pyridyl-N in the apical position (τ = 0.44). The steric crowding in the centrosymmetric molecule is apparent from Figure 4c. There are also three structures with bridging bpe ligands. The structure of $\{Zn[S_2P(OiPr)_2]_2(bpe)\}_n$ (**11**) [36] with a N_2S_2 donor sets resembles the zig-zag polymeric structure of **10**. However, for $\{Zn[S_2P(OR)_2]_2(bpe)\}_n$, for R = iBu (**12**) [37] and R = Cy (**13**) [35], distorted octahedral geometries based on *trans*-N_2S_4 donor sets are observed leading to effectively linear coordination polymers. Particularly noteworthy is the polymeric structure of **13**, the first thus far in this survey featuring bulky cyclohexyl groups. As seen from Figure 4d, the ethene link between the 4-pyridyl rings introduces more space between adjacent zinc centres which readily accommodates the large cyclohexyl rings and thereby, enables the formation of a polymeric chain.

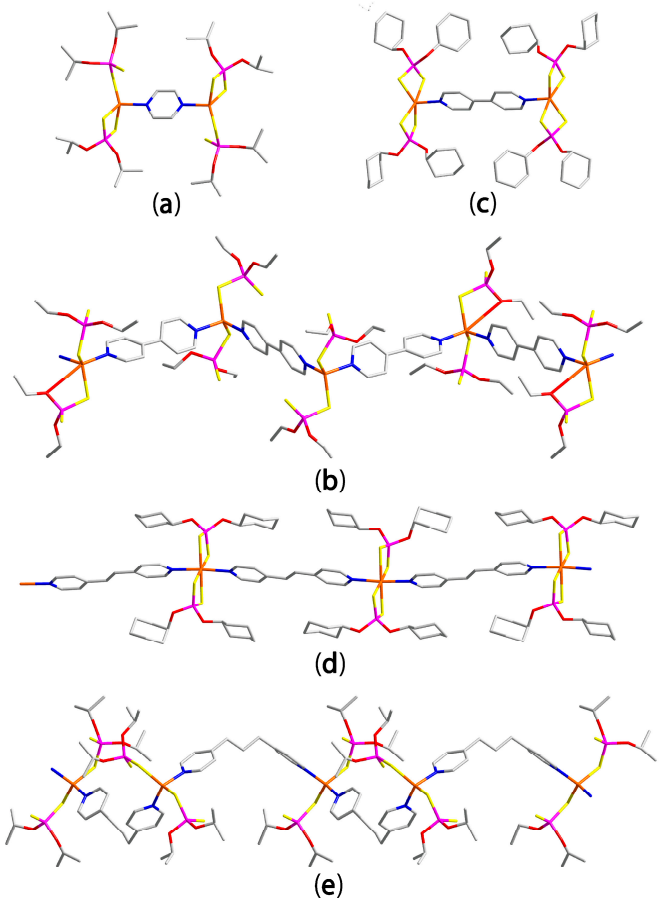

Figure 4. Aggregation in the structures of (**a**) $\{Zn[S_2P(OiPr)_2]_2\}_2(pyr)$ (**7**); (**b**) $\{Zn[S_2P(OEt)_2]_2(bpy)\}_n$ (**8**); (**c**) $\{Zn[S_2P(OCy_2)_2]_2\}_2(bpy)$ (**10**); (**d**) $\{Zn[S_2P(OCy)_2]_2(bpe)\}_n$ (**13**); and (**e**) $[Zn(S_2COiPr)_2(bpp)]_n$ (**19**). Additional colour code: phosphorus, pink.

The next five structures feature the saturated version of the bpe ligand, that is, *trans*-1,2-bis (4-pyridyl)ethane (bpeh), and it is particularly notable that both 2:1 and 1:1 structures were characterised during systematic studies of these molecules. Thus, $\{Zn[S_2P(OiPr_2)_2]_2\}_2(bpeh)$ (**14**) [38] is centrosymmetric and resembles the aggregate shown in Figure 4c. A difference arises in that the NS_4 coordination geometry tends towards trigonal-bipyramidal (τ = 0.58). In the same way, the structures

of $\{Zn[S_2P(OR)_2]_2(bpeh)\}_n$, for R = Et (**15**) [35] and R = iPr (**16**) [35], the 1:1 analogue of **14**, resemble the zig-zag polymer chains illustrated in Figure 4b. Continuing this theme, $\{Zn[S_2P(OiBu)_2]_2(bpeh)\}_n$ (**17**) [39] mimics the linear chain and *trans*-N_2S_4 coordination geometry shown for **12** in Figure 4d. A difference between the bpe- and bpeh-containing structures occurs in the case when R = Cy. Thus, in $\{Zn[S_2P(OCy)_2]_2(bpeh)\}_n$ (**18**) [35], the topology of the chain is zig-zag in contrast to the linear chain found for **13**. This suggests a subtle interplay between the adoption of linear versus zig-zag chains. It is noted the Zn ··· Zn separation in the bpe-containing structure, **13**, is 13.8 Å compared with 13.2 Å in **18**. Thus, a more compact arrangement is found for the zig-zag chain. This is achievable in the case when the bridging ligand is bpeh, as the kink in the molecule alleviates steric hindrance.

There is a single example of a structure with a bridging *trans*-1,2-bis(4-pyridyl)propane (bpp) ligand, namely $\{Zn[S_2P(OiPr)_2]_2(bpp)\}_n$ (**19**) [32]. Each of the two independent zinc atoms in the structure have distorted tetrahedral coordination geometries and, owing to the curved nature of the n-propyl bridge between the 4-pyridyl residues, the resulting coordination polymer has a helical topology as shown in Figure 4e. The following structures to be summarised contain less frequently studied bipyridyl-type molecules.

The ligand, bis(4-pyridyl)disulphide (bpS_2), is bridging in $\{Zn[S_2P(OiPr)_2]_2(bpS_2)\}_n$ (**20**) [32]. In **20**, one dithiophosphate ligand is S-monodentate and the other is S,O-chelating but with the 2n–O separation about 0.9 Å longer than the Zn–S bond length. The N_2OS_2 donor set defines a coordination geometry tending towards square-pyramidal with the value of τ being 0.38. The resultant coordination polymer has a zig-zag topology (glide symmetry) and is illustrated in Figure 5a. A zig-zag coordination polymer is also found in the crystal of $\{Zn[S_2P(OiPr)_2]_2(bpa)\}_n$ (**21**) [32], where bpa is bis(4-pyridyl)amine; the zinc atom exists in a distorted tetrahedral N_2S_2 donor set. The notable characteristic of the bpa ligand is the presence of hydrogen bonding functionality. Indeed, amine-N–H ··· O(alkoxy) hydrogen bonds are formed which serve to link chains into supramolecular layers as shown in Figure 5b.

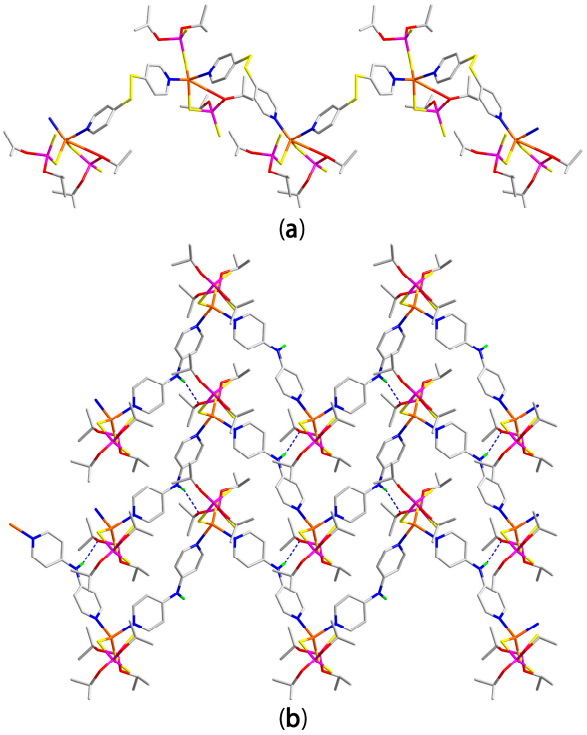

Figure 5. Aggregation in the structures of (**a**) $\{Zn[S_2P(OiPr)_2]_2(bpS_2)\}_n$ (**20**); and (**b**) $\{Zn[S_2P(OiPr)_2]_2(bpa)\}_n$ (**21**). Additional colour code: hydrogen, green. The amine-N–H ··· O(alkoxy) hydrogen bonds in (**b**) are shown as blue dashed lines.

The 1,2-bis(4-pyridylmethylene)hydrazine (4-pyald; 4-pyridylaldazine) ligand is the first example of a bipyridyl-type ligand in this survey with heteroatoms in the bridge linking the 4-pyridyl residues. With four atoms in the link—that is, an all-*trans* CN_2C sequence, separating the 4-pyridyl residues—there is sufficient space to accommodate the bulky cyclohexyl groups in $\{Zn[S_2P(OCy)_2]_2(4\text{-pyald})\}_n$ (**22**) [40], and a zig-zag coordination polymer ensues, Figure 6a. The curious feature of this structure relates to the relative disposition of the sulphur atoms. In the related preceding structures, *trans*-N_2S_4 donor sets were noted but, here the donor set is *cis*-N_2S_4.

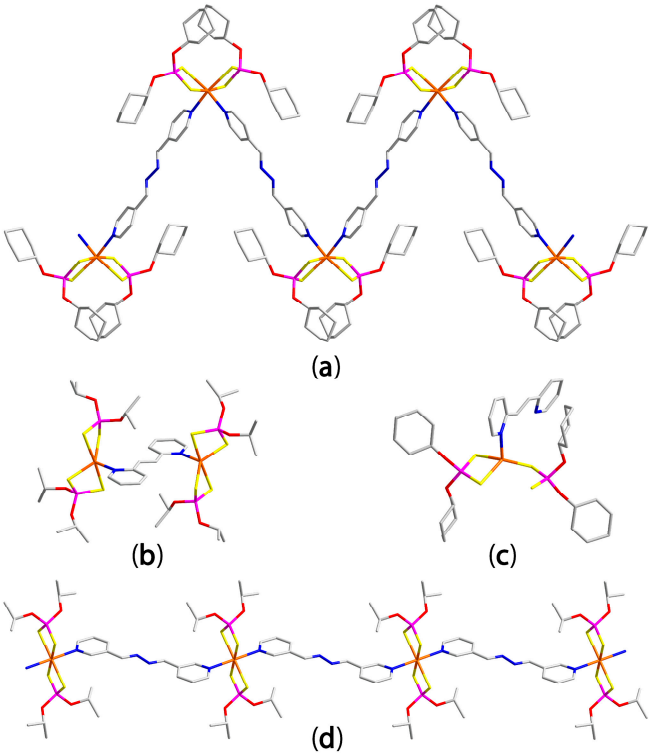

Figure 6. Aggregation in the structures of (**a**) $\{Zn[S_2P(OCy)_2]_2(4\text{-pyald})\}_n$ (**22**); (**b**) $\{Zn[S_2P(OiPr)_2]_2(2\text{-bpe})\}_2$ (**23**); (**c**) $Zn[S_2P(OCy)_2]_2(2\text{-bpe})$ (**24**); and (**d**) $\{Zn[S_2P(OiPr)_2]_2(3\text{-pyald})\}_n$ (**25**).

Thus far, all bipyridyl-type ligands described have had the 4-pyridyl isomer; in the three remaining dithiophosphate structures, isomeric 2-pyridyl and 3-pyridyl species connect zinc atoms. Unlike the polymeric bpe analogue, **11**, the structure of $Zn[S_2P(OiPr)_2]_2(2\text{-bpe})\}_2$ (**23**) [32], where 2-bpe is the 2-pyridyl isomer of bpe, that is *trans*-1,2-bis(4-pyridyl)ethylene, is dimeric, no doubt owing to steric congestion, Figure 6b. In the centrosymmetric molecule, the NS_4 donor set approximates a trigonal-bipyramidal geometry (τ = 0.80) with the less tightly bound sulphur atoms of the asymmetrically coordinating dithiophosphate ligands occupying axial positions (S–Zn–S = 177°). Increasing the steric bulk of the alkoxyl substituents to cyclohexyl means that not even dimerisation can occur. As shown in Figure 6c, the 2-bpe ligand adopts a very rare monodentate coordination mode in the monomeric structure of $Zn[S_2P(OCy)_2]_2(2\text{-bpe})$ (**24**) [32]. The 1,2-bis(3-pyridylmethylene)hydrazine (3-pyald) ligand is the 3-pyridyl isomer of 4-pyald seen in the structure of **22**. In $\{Zn[S_2P(OiPr)_2]_2(3\text{-pyald})\}_n$ (**25**) [41], bridging is observed and a linear coordination polymer is formed, Figure 6d. The distorted *trans*-N_2S_4 coordination geometry is distorted octahedral.

There are single examples each of dithiophosphate analogues where the alkoxy groups are systematically substituted by alkyl groups, that is, giving dithiophosphonate and dithiophosphinate, Figure 1. In $\{Zn[S_2P(4\text{-MePh})OMe]_2(bpeh)\}_n$ (**26**) [42], a tetrahedral N_2S_2 donor set and zig-zag coordination polymer is seen as in **15**, **16** and **18**. Finally, in $\{Zn[S_2P(iBu)_2]_2(bpy)\}_n$ (**27**) [43],

an octahedral N_2S_4 donor set and linear coordination polymer is observed. This is in contrast to the zig-zag polymers observed in the bpy analogues **8** and **9** but, in accord with the linear polymers seen in the bpe (**12**) and bpeh (**17**) analogues perhaps suggesting a propensity for this type of polymer topology for isobutyl substituents.

3.3. Zinc Dithiocarbamate Structures

There are 30 dithiocarbamate structures, that is, **28**–**57** [44–66], to be described in this section, Table 1. While the majority of the structures conform to already-observed motifs, there are a number of unexpected modes of coordination for the bipyridyl-type ligands, often in the presence of dithiocarbamate ligands functionalised with groups capable of forming hydrogen bonding interactions. Hence, this section is divided into discussions of structures not capable of forming hydrogen bonds and those that are.

3.3.1. Zinc Dithiocarbamate Structures Not Capable of Forming Hydrogen Bonds

The most unexpected structure to be described in this section is monomeric $Zn(S_2CNEt_2)_2(bpy)$ (**28**) [44] as, rather than bridging, the bpy molecule coordinates in the monodentate mode: see Figure 7a. With a value of $\tau = 0.51$, the NS_4 donor set is nearly perfectly intermediate between square-pyramidal and trigonal-pyramidal. The remaining structures involving bpy, **29**–**36** [45–52] have this ligand in the expected bridging mode: see Table 1. The prototype structure of the majority of these $[Zn(S_2CNR_2)_2]_2(bpy)$ structures is the R = Me derivative, **29** [45], shown in Figure 7b. The molecule in **29** is located about a centre of inversion indicating the dihedral angle between the pyridyl rings of bpy is 0°. Identical symmetry is found in the R = nPr (**31**) [44], iPr (**32**) [48], iBu (**33**) [49] and CH_2Ph (**34**) [50] structures. There are three variations. In $\{Zn[S_2CN(CH_2)_4]_2\}_2(bpy)$ (**35**) [51], the molecule is situated about a site of symmetry 222. In $[Zn(S_2CNEt_2)_2]_2(bpy)$ (**30**) [46,47], there are two independent molecules in the asymmetric unit: one where the ZnNNZn vector is coincident with the two-fold axis, and the other where the two-fold axis is perpendicular to the ZnNNZn vector. In a sense, the structure of $\{Zn[S_2CN(CH_2)_5]_2\}_2(bpy)$ (**36**) [52] represents a synthesis of the above in that there are two independent molecules, one situated about a centre of inversion and the other molecule having 2-fold symmetry coincident with the ZnNNZn axis. In the non-centrosymmetric molecules, the range of dihedral angles between the pyridyl rings of bpy is 25 to 39° for the molecule with two-fold axes coincident with the ZnNNZn vector in **30** and the molecule in 222-symmetric **35**, respectively. In each of **29**–**36**, the donor set about the zinc atom is defined by NS_4 atoms. The coordination geometries range from almost square-pyramidal for the R = nPr (**31**) derivative with $\tau = 0.11$ to approaching trigonal-bipyramidal for the R = CH_2Ph (**34**) derivative with $\tau = 0.70$.

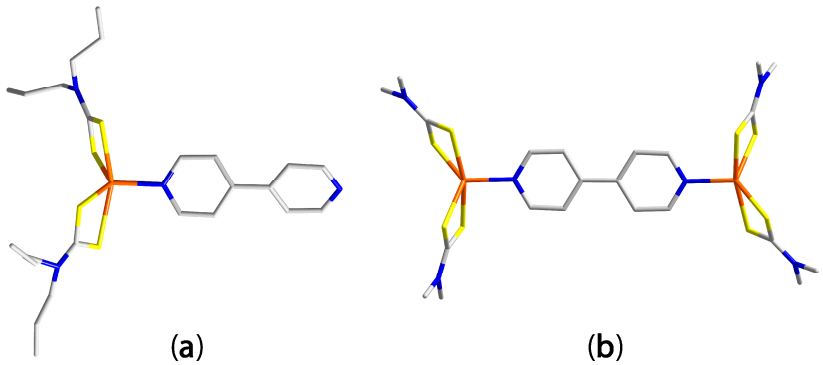

Figure 7. Aggregation in the structures of (**a**) $Zn(S_2CNEt_2)_2(bpy)$ (**28**) and (**b**) $[Zn(S_2CNMe_2)_2]_2(bpy)$ (**29**).

The four zinc dithiocarbamate species with bpe, that is **37**–**40** [53–56], Table 1, also adopt the same dimeric motif as illustrated in Figure 7a; the bpe is planar or close to planar in each case. The NS_4 donor

sets tend to be closer to square-pyramidal in three examples, that is τ ranges from 0.13 for the R = Et (**40**) to 0.39 for R = Me (**37**) derivatives, while NS_4 is closer to trigonal-bipyramidal for the R = Et (**38**) species, with τ = 0.56. While no molecular symmetry is event for **37**–**39**, the binuclear molecule in **40** is disposed about a centre of inversion. The structure of **40** is of particular interest as it was isolated as a 1:1 lattice adduct with a non-coordinating molecule of bpe during unsuccessful attempts to encourage polymer formation by having an excess of bpe in solution during crystallisation [56]. The final structure in this section also follows the motif shown in Figure 7b, that is, binuclear $\{Zn[S_2CN(nPr)_2]_2\}_2$(bpeh) (**41**) [57]. The molecule has no symmetry and the NS_4 donor set approaches trigonal-bipyramidal with τ values of 0.64 and 0.72 for the independent zinc atoms.

3.3.2. Zinc Dithiocarbamate Structures Capable of Forming Hydrogen Bonds

Many of the structures described in this section conform to the motifs established earlier in this review. However, with hydrogen bonding functionality, supramolecular aggregation between the aggregates usually occurs leading to supramolecular architectures of higher dimensionality.

The first three structures to be discussed in this category have dialkyldithiocarbamate ligands coupled with bipyridyl-type ligands that have hydrogen bonding potential, for example *N*,*N*′-bis(pyridin-4-ylmethyl)ethanediamide (4-pdaO). In $[Zn(S_2CNEt_2)_2]_2$(4-pdaO) (**42**) [58], the binuclear molecule is disposed about a centre of inversion with the crank-shaft shape of the 4-pdaO bridge leading to the distinctive kink in the molecule, Figure 8a. The NS_4 donor set approximates a square-pyramid as indicated by the value of τ = 0.20. The next two molecules contain the 3-pyridyl isomer of 4-pdaO, *N*,*N*′-bis(pyridin-3-ylmethyl)ethanediamide (3-pdaO) and two distinctive conformations are observed. In $[Zn(S_2CNMe_2)_2]_2$(3-pdaO) (**43**) [59], isolated as a di-dimethylformamide (DMF) solvate, a similar centrosymmetric conformation for the 3-pdaO molecule is seen as for **42**. Similarly, the value of τ = 18 indicates the NS_4 coordination geometry is based on a square-pyramid. The co-crystallised DMF molecules are associated with the binuclear molecule via amide-N–H ··· O(DMF) hydrogen bonds, Figure 8b, so no further supramolecular association is possible in the crystals, at least via hydrogen bonding. A major conformational change is evident for the 3-pdaO molecule in $\{Zn[S_2CN(nPr_2)]_2\}_2$(3-pdaO) (**44**) [59]. As seen from Figure 8c, the bridging 3-pdaO molecule has a U-shape; the molecule has 2-fold symmetry. In contrast to **42**, the NS_4 coordination geometry in **43** is based on a trigonal-pyramid with τ = 0.76. While such remarkable differences in conformation may seem incongruent, computational chemistry performed on 3-pdaO show that the energy difference between the extended form, where the 3-pyridyl rings are anti-periplanar, and the curved form, where the rings are syn-periplanar, is less than 1 kcal/mol [71]. This observation highlights the conformational flexibility of this class of molecule and their related thioamide derivatives [72]. A consequence of the U-shape of the molecule in **43** is that rows of alternating oppositely orientated molecules are linked by amide-N–H ··· O(amide) hydrogen bonds leading to a supramolecular tape, as in Figure 8d.

The structure of $\{Zn[S_2CN(CH_2CH_2OH)_2]_2\}_2$(pyr) has been determined solvent-free (**45**), as well as its di-dioxane solvate (**46**) [60]. The molecular structures resemble the binuclear aggregate shown in Figure 7b. In **45**, the molecule is disposed about a centre of inversion and the same is true for each of the two independent molecules in **46**. The values of τ value from 0.19 (**45**) to 0.26 and 0.40 (**46**) indicating a tendency towards square-pyramidal. In each of **45** and **46** there is extensive hydroxyl-O–H ··· O(hydroxyl) hydrogen bonding, involved all hydroxyl groups as acceptors and donors, leading to a three-dimensional architecture, Figure 9. As discussed in the original publication, there are no solvent accessible voids in **45** and the key crystal indicators, that is density (1.709 compared with 1.570 g/cm^3) and packing efficiency (74.9 compared with 71.6%), suggest that **46** represents a less efficient packing arrangement, owing to the presence of dioxane molecules. Consistent with this is the lack of strong intermolecular interactions between the host lattice and the dioxane molecules resident in the channels. The rationale for the formation of **46** rests with the observation that owing to the high

boiling point of dioxane, the dioxane molecules were trapped in the crystal under the conditions of specific crystallisation experiment [60].

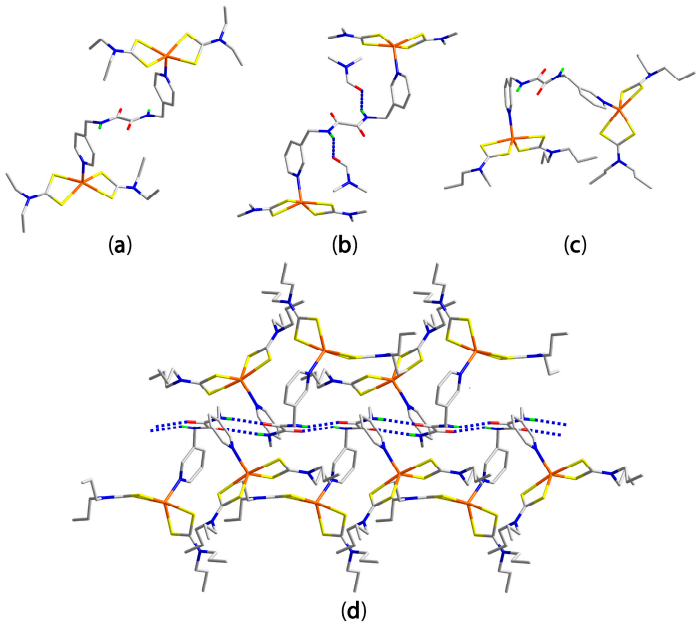

Figure 8. Aggregation in the structures of (**a**) $[Zn(S_2CNEt)_2]_2$(4-pdaO) (**42**); (**b**) $[Zn(S_2CNMe)_2]_2$(3-pdaO).2-di-dimethylformamide (DMF) (**43**); (**c**) $\{Zn[S_2CN(nPr_2)]_2\}_2$(3-pdaO) (**44**); and (**d**) supramolecular tape mediated by amide-N–H ··· O(amide) hydrogen bonds (blue dashed lines) in **44**.

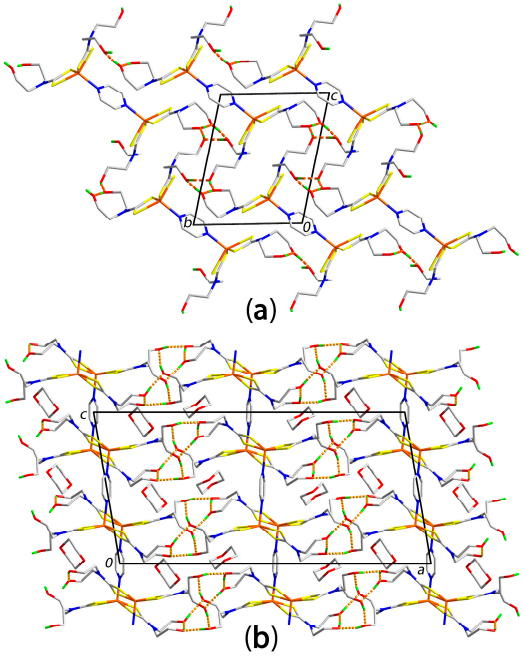

Figure 9. Three-dimensional supramolecular aggregation in the structures of (**a**) $\{Zn[S_2CN(CH_2CH_2OH)_2]_2\}_2$(pyr) (**45**); and (**b**) $\{Zn[S_2CN(CH_2CH_2OH)_2]_2\}_2$(pyr).2dioxane (**46**). The hydroxyl-O–H ··· O(hydroxyl) hydrogen bonds are shown as orange dashed lines.

The next four structures, having bridging bpy ligands, resemble the molecule shown in Figure 7b. As established above, there are no apparent patterns in the symmetry of the molecules nor in the adoption of coordination geometry. In $\{Zn[S_2CN(Me)CH_2CH_2OH]_2\}_2$(bpy) (**47**) [61], the molecule is

disposed about a centre of inversion and the zinc atom has an intermediate coordination geometry between the two extremes ($\tau = 0.54$). By contrast, the ethyl analogue, {Zn[S_2CN(Et)CH_2CH_2OH]$_2$}$_2$(bpy) (**48**) [61], is non-symmetric with coordination geometries close to square-pyramidal ($\tau = 0.21$) and intermediate between this and trigonal-bipyramidal ($\tau = 0.51$) for the second zinc atom. However, the di-methanol solvate of **48**, Zn[S_2CN(Et)CH_2CH_2OH]$_2$}$_2$(bpy).2CH_3OH (**49**) [61], is centrosymmetric with a coordination geometry approaching trigonal-bipyramidal ($\tau = 0.62$). In the fourth structure of this series, with a symmetrically substituted dithiocarbamate ligand, {Zn[S_2CN(CH_2CH_2OH)$_2$]$_2$}$_2$(bpy) (**50**) [61], there is no molecular symmetry and with τ values of 0.34 and 0.54, the coordination geometries follow the pattern as for **48**. The molecular packing in each of the four crystals is quite distinct. In the crystal of **47**, hydroxyl-O–H ··· O(hydroxyl) hydrogen bonding connects molecules into supramolecular layers via eight-membered {. . . H-O}$_4$ synthons. From Figure 10a, left, it is apparent that the layers have rather large voids and, indeed, perpendicularly inclined layers interpenetrate to form a three-dimensional architecture, shown in Figure 10a, right. Supramolecular layers are also formed in the R = Et analogue, **48**. The assembly is distinct, as in Figure 10b, left, from that in **47**. Centrosymmetrically related layers are connected via further hydroxyl-O–H ··· O(hydroxyl) hydrogen bonding to form double layers, shown in Figure 10b, right. The key supramolecular synthon is a 12-membered {. . . H-O}$_6$ ring connected to two further exocyclic hydroxyl-O–H ··· O(hydroxyl) hydrogen bonds. The presence of solvent methanol in **49** effectively blocks off half of the hydrogen bonding capacity of the hydroxyethyl groups owing to the formation of methanol-O–H ··· O(hydroxyl) hydrogen bonds. The remaining hydroxyethyl groups form hydroxyl-O–H ··· O(hydroxyl) hydrogen bonds to generate the supramolecular ladder shown in Figure 10c. In **50**, where both N-bound R group carry hydrogen bonding potential, a three-dimensional architecture ensues, Figure 10d. It is of interest that one of the hydroxyl groups in **50** does not form hydroxyl-O–H ··· O(hydroxyl) hydrogen bonds but hydroxyl-O–H ··· S hydrogen bonds instead. The propensity of such hydrogen bonds in $^-S_2CNCH_2CH_2OH$ dithiocarbamate ligands has been summarised recently, a summary which suggested these are relatively common in the structural chemistry of these ligands [73].

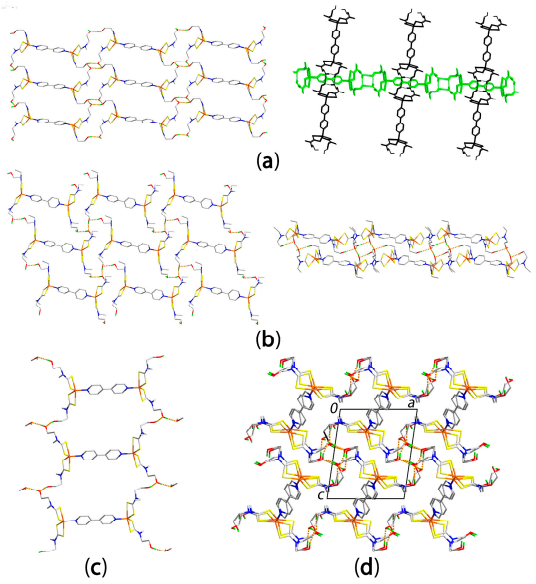

Figure 10. Supramolecular aggregation sustained by hydroxyl-O–H ··· O(hydroxyl) hydrogen bonding in the crystals of (**a**) {Zn[S_2CN(Me)CH_2CH_2OH]$_2$}$_2$(bpy) (**47**) showing a layer (left) and partial two-fold inclined interpenetration of two layers; (**b**) {Zn[S_2CN(Et)CH_2CH_2OH]$_2$}$_2$(bpy) (**48**) showing a layer (left) and the double-layer; (**c**) {Zn[S_2CN(Et)CH_2CH_2OH]$_2$}$_2$(bpy).2CH_3OH (**49**) showing a ladder; and (**d**) {Zn[S_2CN(CH_2CH_2OH)$_2$]$_2$}$_2$(bpy) (**50**) showing the three-dimensional architecture.

The next structure to be described was isolated from frustrated experiments to force the formation of a coordination polymer by having an excess of bpy in the crystallisation. Thus, $Zn[S_2CN(iPr)CH_2CH_2OH]_2(bpy).(bpy)_{0.5}$ (**51**) [62] has monodentate and uncoordinated bpy in the lattice. A view of the zinc-containing molecule is shown in Figure 11a. The familiar NS_4 donor set is noted and this approaches a trigonal-bipyramidal geometry as judged by the value of $\tau = 0.64$. There is a considerable twist in the coordinated bpy molecule of 28° which compares with 0° for the uncoordinated, centrosymmetric molecule.

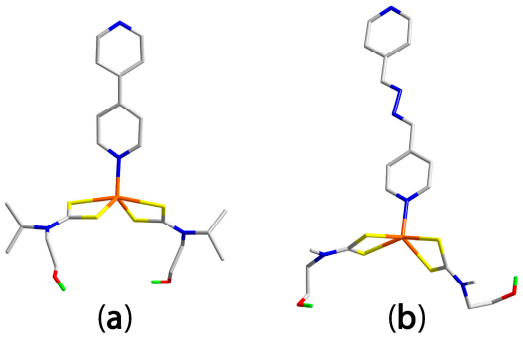

Figure 11. Aggregation in the structures of (**a**) $Zn[S_2CN(iPr)CH_2CH_2OH]_2(bpy).(bpy)_{0.5}$ (**51**); and (**b**) $Zn[S_2CN(Me)CH_2CH_2OH]_2$(4-pyald) (**52**).

In the crystal, rather large 28-membered $\{\ldots HOC_2NCSZnSCNC_2O\}_2$ synthons are formed via hydroxyl-O–H $\cdots$ O(hydroxyl) hydrogen bonds as molecules arrange in a head-to-head fashion. There are two free hydroxyl-H atoms associated with this ring and they connect to the non-coordinating end of the coordinated bpy molecules via hydroxyl-O–H $\cdots$ N(pyridyl) hydrogen bonds to generate the two-dimensional array shown in Figure 12a. Weak non-covalent interactions assemble layers into a three-dimensional architecture and the connections between the host lattice and non-coordinating bpy molecules are of the type bpy-C–H$\cdots$O(hydroxyl) interactions.

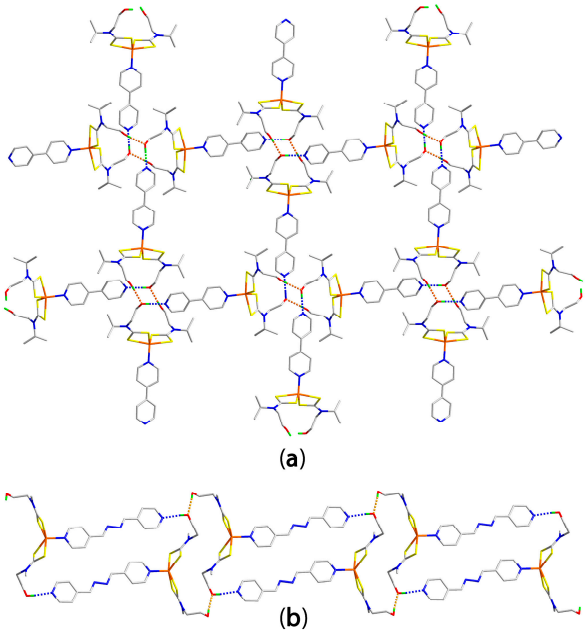

Figure 12. Supramolecular aggregation sustained by hydroxyl-O–H $\cdots$ O(hydroxyl) and hydroxyl-O–H $\cdots$ N(pyridyl) hydrogen bonding in the crystals of (**a**) $Zn[S_2CN(iPr)CH_2CH_2OH]_2(bpy).(bpy)_{0.5}$ (**51**); and (**b**) $Zn[S_2CN(Me)CH_2CH_2OH]_2$(4-pyald) (**52**).

There is a second structure with a monodentate bipyridyl-type molecule, namely $Zn[S_2CN(Me)CH_2CH_2OH]_2$(4-pyald) (**52**) [63], shown in Figure 11b. The NS_4 donor set defines a distorted square-pyramidal geometry (τ = 0.32). In the crystal, hydroxyl-O–H ··· O(hydroxyl) and hydroxyl-O–H ··· N(pyridyl) hydrogen bonds combine to stabilise a double-chain, Figure 12b. The 28-membered { ... $HOC_2NCSZnSCNC_2O\}_2$ synthons seen in **51** feature in the crystal of **52** also. Indeed, this synthon occurs in a fascinating pair of structures to be discussed next which combine zinc-containing molecules and bridging bipyridyl-type ligands, each with hydrogen bonding functionality.

The commonly NS_4 donor sets for zinc dithiocarbamates are found in the structures of $Zn[S_2CN(Me)CH_2CH_2OH]_2$(3-pdaO) (**53**) [64] and $Zn[S_2CN(Me)CH_2CH_2OH]_2$(3-pdaOt) (**54**) where 3-pdaOt, N-(pyridin-2-ylmethyl)-N′-(pyridin-3-ylmethyl)ethanediimidic acid, is the hydroxyl-imine tautomer of 3-pdaO, shown in Figure 13a. The values of τ for the centrosymmetric molecules in **53**, 0.66, and **54**, 0.54, suggest tendencies towards trigonal-bipyramidal. The molecular packing for both molecules is very similar and discussion will focus on that in the crystal of **54**. Here, molecules assemble via hydroxyl-O–H ··· O(hydroxyl) hydrogen bonds to form 28-membered { ... $HOC_2NCSZnSCNC_2O\}_2$ synthons and supramolecular chains, Figure 13b. In this case, the large rings are threaded by centrosymmetrically related chains to form inter-woven coordination polymers, as shown in Figure 13c. The links between the individual chains in **54** are of the type hydroxyl-O–H ··· N(imine), and in **53**, of the type hydroxyl-O–H ··· O(amide) [64]. The next two structures to be discussed contain sulphur analogues of 3-pdaO.

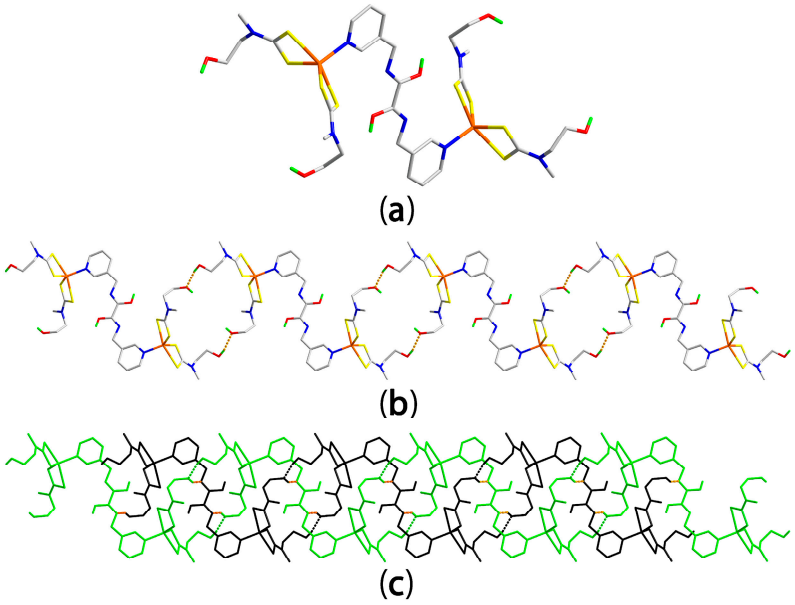

Figure 13. (**a**) Molecular structure of $Zn[S_2CN(Me)CH_2CH_2OH]_2$(3-pdaOt) (**54**); (**b**) supramolecular chain sustained by hydroxyl-O–H ··· O(hydroxyl) hydrogen bonding; and (**c**) schematic of the inter-woven coordination polymer with individual chains coloured black and green and with hydroxyl-O–H ··· N(imine) hydrogen bonds (orange dashed lines) between the chains shown in (**b**).

The familiar distorted NS_4 coordination geometries are found in each of centrosymmetric $Zn[S_2CN(Me)CH_2CH_2OH]_2$(3-pdaS) (**55**), Figure 14, isolated as a DMF di-solvate, and $Zn[S_2CN(Me)CH_2CH_2OH]_2$(3-pdaS) (**56**), whichwas co-crystallised serendipitously with two equivalents of S_8 owing to partial desulphurisation during crystallisation [65]. The values of τ are 0.46 and 0.08, respectively, suggesting the coordination geometry in **56** is relatively closely based on a square-pyramid.

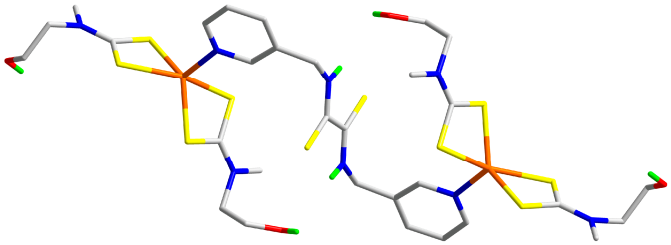

Figure 14. Molecular structure of $Zn[S_2CN(Me)CH_2CH_2OH]_2(3\text{-pdaS})$ in (**55**).

In the molecular packing of **55**, half of the hydroxyl groups form hydroxyl-O–H ··· O(DMF) hydrogen bonds and the remaining hydroxyl groups form hydroxyl-O–H ··· O(hydroxyl) hydrogen bonds to form a supramolecular ladder, via the 28-membered { ... $HOC_2NCSZnSCNC_2O\}_2$ synthons commented upon above, Figure 15a. Additional stabilisation to the supramolecular one-dimensional chain is provided by amide-N–H ··· O(DMF) and amide-N–H ··· S(thioamide) hydrogen bonds, not shown. The key feature of the supramolecular aggregation in **56** is the forming of planar { ... $HO\}_4$ synthons contributed to by four separate molecules and which extend laterally to form a two-dimensional array resembling that shown for **48** in Figure 10b. Layers are connected into a three-dimensional architecture by amide-N–H ··· S(amide) hydrogen bonds to define channels in which reside the S_8 molecules, Figure 15b.

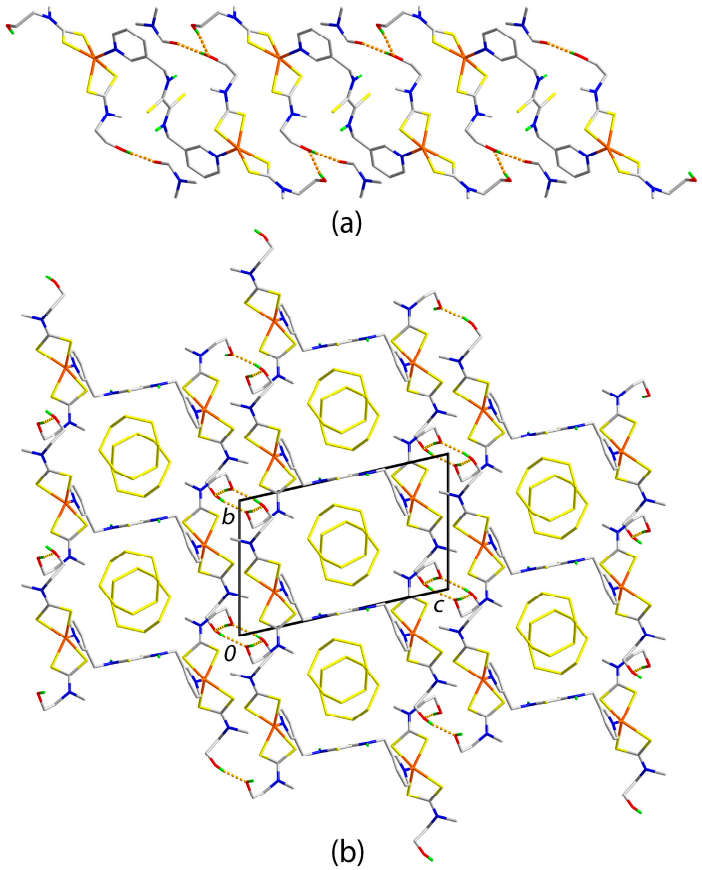

Figure 15. Supramolecular aggregation sustained by hydroxyl-O–H ··· O(hydroxyl) hydrogen bonding in the crystals of (**a**) $Zn[S_2CN(Me)CH_2CH_2OH]_2(3\text{-pdaS}).2DMF$ (**55**) with additional by hydroxyl-O–H ··· O(DMF) hydrogen bonding; and (**b**) $Zn[S_2CN(Me)CH_2CH_2OH]_2(3\text{-pdaS}).2S_8$ (**56**) showing the occupancy of channels by S_8 molecules.

The final zinc-containing structure to be described is one containing the 2,4,6-tris (pyridin-2-yl)-1,3,5-triazine ligand abbreviated as triazine. The molecular structure of $Zn[S_2CN(Me)CH_2CH_2OH]_2$(triazine).1.5(dioxane) (**57**) [66] is noteworthy for being the only example having monodentate-coordinating dithiocarbamate ligands, as in Figure 16a. This arises as the triazine molecule is tridentate, forming bonds to zinc via a triazine- and two pyridyl-nitrogen atoms. The resulting N_3S_2 donor set is very close to a square-pyramid with $\tau = 0.07$ and with a sulphur atom occupying the apical position. In the molecular packing, molecules are arranged in rows and are held in place by hydroxyl-O–H ··· N(triazine), N(pyridyl) hydrogen bonds, and these are connected into a two-dimensional array via hydroxyl-O–H ··· S(dithiocarbamate) hydrogen bonds as shown in Figure 16b.

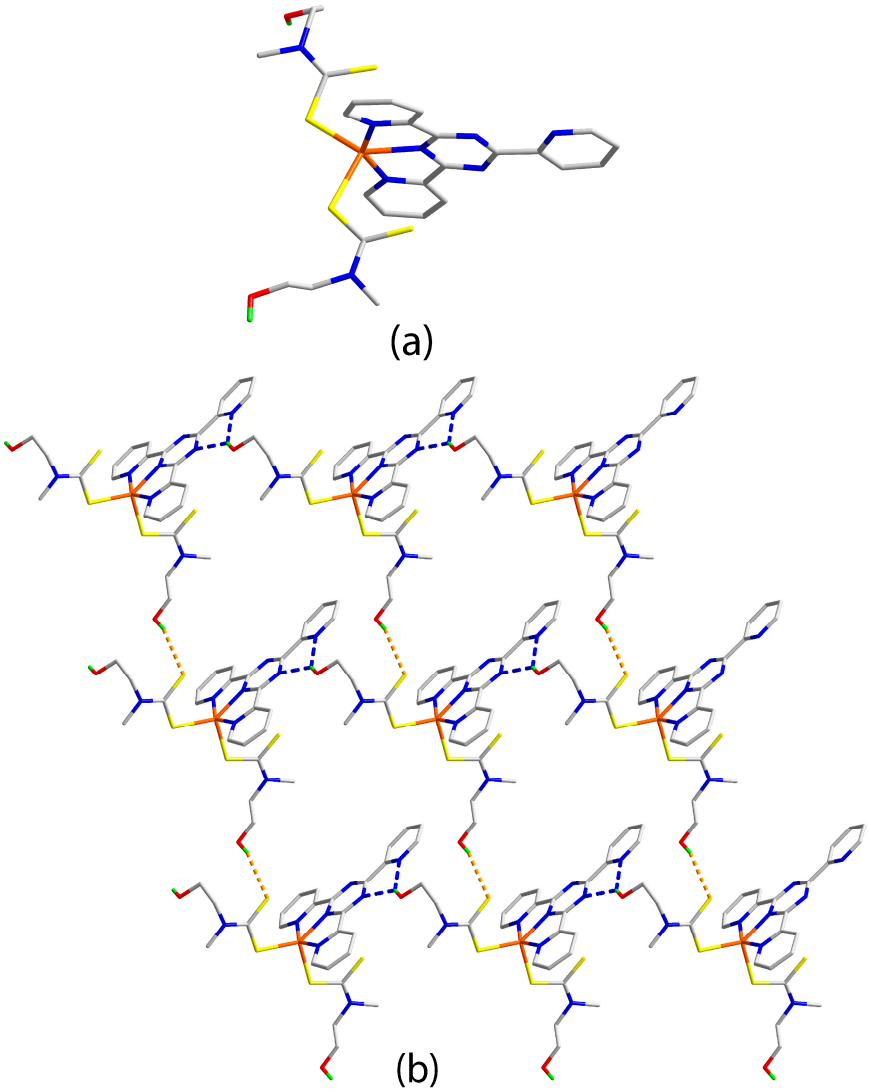

Figure 16. Images for $Zn[S_2CN(Me)CH_2CH_2OH]_2$(triazine)·1.5(dioxane) (**57**): (**a**) molecular structure; and (**b**) supramolecular aggregation sustained by hydroxyl-O–H ··· S(dithiocarbamate) and hydroxyl-O–H ··· S(triazine, pyridyl) hydrogen bonding shown as orange and blue dashed lines, respectively.

3.4. Cadmium Xanthate Structure

There is a sole example of a cadmium xanthate structure, $[Cd(S_2COiPr)_2(bpy)]_n$ (**58**) [74], making xanthates the least represented of the conventional 1,1-dithiolate ligands included in this review;

data for all 31 cadmium structures, that is, **58**–**88** [62,74–92], are listed in Table 2. There are two independent formula units in the crystal and each of these is disposed about a two-fold axis of asymmetry with the cadmium and nitrogen atoms lying on the axis. Each independent formula unit self-associates to form a linear chain. The conformations of the bridging bpy molecules distinguish the structures. In one repeat unit, the bpy is effectively planar, with the dihedral angle between the two rings being 3°, Figure 17, while, in the other residue, the rings are twisted forming a dihedral angle of 26°. This observation highlights the conformational flexibility of the bpy molecule as noted in the zinc structures described above.

Table 2. Summary of the general features of cadmium structures **58**–**88** [62,74–92].

Compound	R/R′	N-Ligand	Donor Set	Motif	Ref.
58	iPr	bpy	N_2S_4	linear chain	[74]
59	Me	bpy	N_2S_4	zig-zag chain	[75]
60	Et	bpy	N_2S_4	linear chain	[76]
61	iPr	bpy	N_2S_4	linear chain	[77]
62	Cy	bpy	N_2S_4	linear chain	[77]
63	iPr	bpe	N_2S_4	linear chain	[77]
64	Cy	bpe	N_2S_4	linear chain	[77]
65	iPr	bpeh	N_2S_4	linear chain	[77]
66	iPr	dpp	N_2S_4	linear chain	[77]
67 [1]	Cy	dpp	N_2S_4	dimer	[77]
68	iPr	bpS_2	N_2S_4	linear chain	[77]
69	iPr	4-pyald	N_2S_4	linear chain	[78]
70	iPr	3-pyald	N_2S_4	linear chain	[78]
71 [1]	Cy	3-pyald	N_2S_4	linear chain	[79]
72	iPr	2-pyald	N_2S_4	dimer	[78]
73	iPr	2-bpe	N_2S_4	linear chain	[77]
74	Cy	2-bpe	N_2S_4	linear chain	[77]
75	Me, 4-MeOPh	bpy	N_2S_4	linear chain	[80]
76	Et, 4-MeOPh	bpy	N_2S_4	linear chain	[81]
77	Me, 4-MeOPh	bpe	N_2S_4	zig-zag chain	[82]
78	Me, 4-MeOPh	dpeh	N_2S_4	zig-zag chain	[83]
79	Me, 4-MeOPh	dpp	N_2S_4	zig-zag chain	[84]
80	iBu	bpy	N_2S_4	linear chain	[85]
81	CH_2Ph	bpy	N_2S_4	linear chain	[86]
82	Et	bpe	N_2S_4	linear chain	[87]
83	Et	bpeh	N_2S_4	linear chain	[88]
84	nPr	2-pyald	N_2S_4	dimeric	[89]
85 [2]	iPr, CH_2CH_2OH	bpy	NS_4	monomeric	[62]
86 [3]	iPr, CH_2CH_2OH	bpe	N_2S_4	dimeric	[90]
87	nPr, CH_2CH_2OH	4-pyald	N_2S_4	monomeric	[91]
88 [4]	iPr, CH_2CH_2OH	3-pyald	N_3S_2	dimeric	[92]

[1] Chloroform di-solvate; [2] Co-crystallised with half an uncoordinated bpy molecule; [3] Acetonitrile tetra-solvate; [4] Dihydrate.

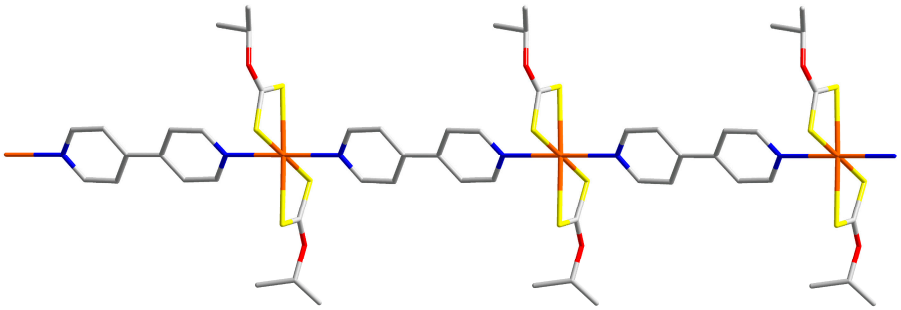

Figure 17. Aggregation in $[Cd(S_2COiPr)_2(bpy)]_n$ (**58**).

3.5. Cadmium Dithiophosphate and Related Structures

By far the most numerous cadmium-containing structures covered in this survey are the dithiophosphates, which have been the subject of a number of systematic studies. There are four structures featuring bridging bpy ligands, $\{Cd[S_2P(OR)_2]_2(bpy)\}_n$ for R = Me (**59**) [75], Et (**60**) [76], iPr (**61**) [77] and Cy (**62**) [77]. All structures present different crystallographic symmetry. Thus, in **59** the bpy ligand is disposed about a centre of inversion, in **60** the cadmium atom is located on a centre of symmetry, for **61** both bpy and cadmium are disposed about centres of inversion whereas for **62**, the cadmium and nitrogen atoms lie on a 2-fold axis of symmetry. In **59**–**61**, the bpy molecules are planar or effectively planar but, in **63** the dihedral angle of 50° between the rings indicates a significant twist. A common feature of the four structures is the N_2S_4 donor set for cadmium, as the dithiophosphate ligands adopt a symmetrically cheating mode, but this has a *cis*-disposition in **59**, leading to a zig-zag chain, Figure 18a, whereas *trans*-N_2S_4 geometries are found in **60**–**62** leading to linear topologies for the resultant coordination polymers, illustrated for **62** in Figure 18b. Linear coordination polymers and *trans*-N_2S_4 donor sets are also found in each of $\{Cd[S_2P(OiPr)_2]_2(bpe)\}_n$ (**63**) $\{Cd[S_2P(OCy)_2]_2(bpe)\}_n$ (**64**) and $\{Cd[S_2P(OiPr)_2]_2(bpeh)\}_n$ (**65**) [77]. While neither of **63** and **64** have crystallographic symmetry, each of the two independent repeat units in **65** have the cadmium atom lying on a centre of symmetry and the bpy molecule lying about a centre of inversion; independent repeat unit self-associate to form independent chains.

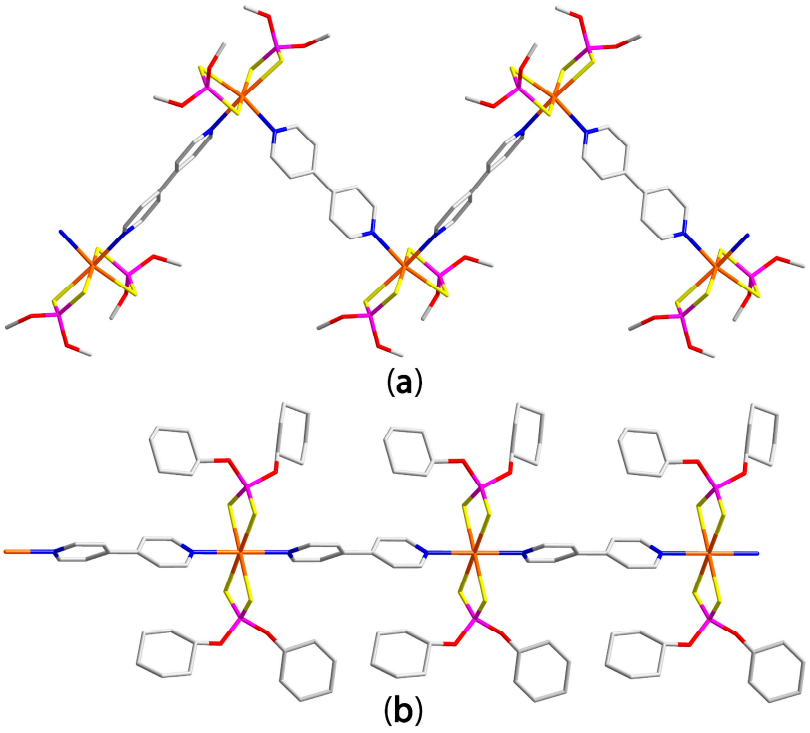

Figure 18. Aggregation in the crystals of (**a**) $\{Cd[S_2P(OMe)_2]_2(bpy)\}_n$ (**59**); and $\{Cd[S_2P(OCy)_2]_2(bpy)\}_n$ (**62**).

There are two structures available with the dpp ligand and the supramolecular aggregation in these are dictated by steric effects. In $\{Cd[S_2P(OiPr)_2]_2(bpp)\}_n$ (**66**) [77], with the cadmium atom lying on a 2-fold axis of symmetry and with the dpp bisected by a 2-fold axis of symmetry, a *cis*-N_2S_4 donor set is found resulting in a linear coordination polymer with characteristic arches owing to the conformation of the dpp ligand, Figure 19a. A similar *cis*-N_2S_4 donor set and arched conformation is found in the structure of $\{Cd[S_2P(OCy)_2]_2(bpp)\}_2$ (**67**) [77], but not the formation of a coordination polymer owing to the steric bulk of the cyclohexyl groups. Instead, a centrosymmetric dimeric aggregate as shown in Figure 19b. In $\{Cd[S_2P(OiPr)_2]_2(bpS_2)\}_n$ (**68**) [77], which is devoid of crystallographic symmetry,

a linear coordination polymer is formed. As seen in Figure 19c, this topology resembles that found for **66** illustrated in Figure 19a. The structures of $\{Cd[S_2P(OiPr)_2]_2(4\text{-pyald})\}_n$ (**69**) and the 3-pyald analogue (**70**) [78] share common features in terms of symmetry (the cadmium atom lies on a centre of symmetry and the 4-pyald molecule lies about a centre of inversion), *trans*-N_2S_4 coordination geometry which defines an octahedron and linear topology for the resultant coordination polymer compared with Figure 18b. A similar description pertains for $\{Cd[S_2P(OCy)_2]_2(4\text{-pyald})\}_n$ (**71**) [79] but, in this case only the cadmium atom lies on a centre of inversion. A different motif is formed when reactions are conducted with the isomeric 2-pyald ligand. As shown in Figure 19d, all four nitrogen atoms of 2-pyald are employed in coordination to cadmium, which exists within a *cis*-N_2S_4 donor set in the centrosymmetric dimer, $\{Cd[S_2P(OiPr)_2]_2(2\text{-pyald})\}_2$ (**72**) [78]. The final two structures are also 2-pyridyl isomers of the more commonly explored bpe ligand. In both $\{Cd[S_2P(OR)_2]_2(2\text{-bpe})\}_n$ for R = iPr (**73**) [79], Figure 19e, and Cy (**74**) [77], the cadmium (within *trans*-N_2S_4 donor sets) and 2-bpe molecules are disposed on/about centres of inversion. Linear coordination polymers are formed as the chelation observed in **72** is no longer possible, thereby making available additional coordination sites for bridging.

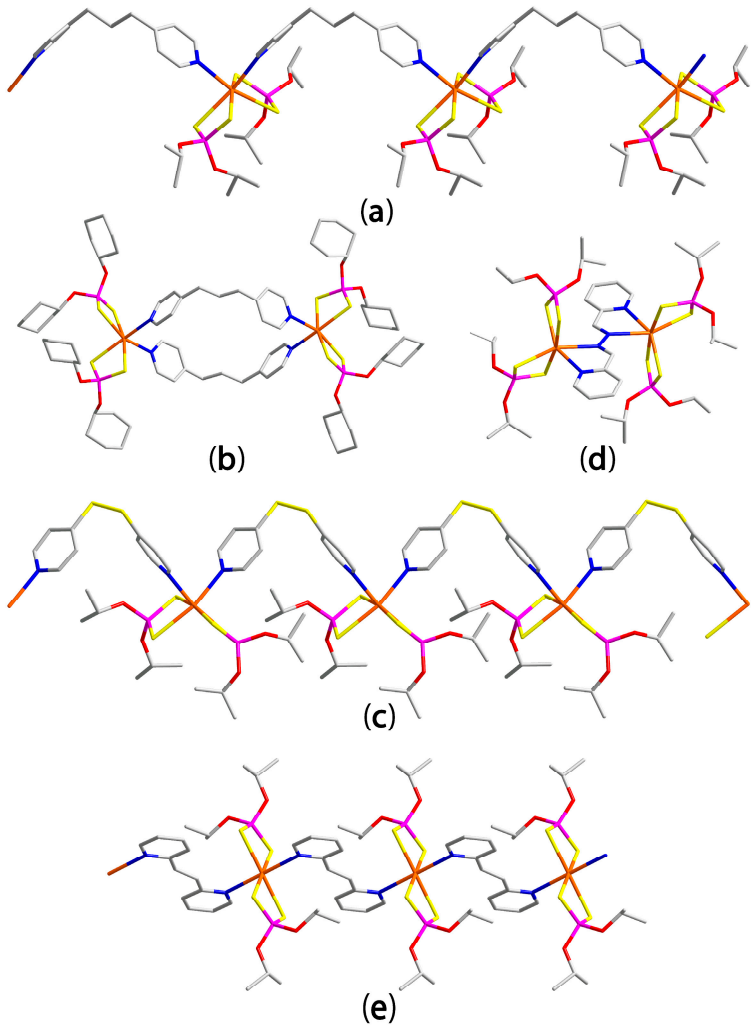

Figure 19. Aggregation in the crystals of (**a**) $\{Cd[S_2P(OiPr)_2]_2(bpp)\}_n$ (**66**); (**b**) $\{Cd[S_2P(OCy)_2]_2(bpp)\}_2$ (**67**); (**c**) $\{Cd[S_2P(OiPr)_2]_2(bpS_2)\}_n$ (**68**); (**d**) $\{Cd[S_2P(OiPr)_2]_2(2\text{-pyald})\}_2$ (**72**); and (**e**) $Cd[S_2P(OiPr)_2]_2(2\text{-bpe})\}_n$ (**73**).

There are five dithiophosphonate structures and one example of a dithiophosphinate structure available in the CSD [2] and these uniformly are one-dimensional coordination polymers but, with distinct topologies. The structures of two bpy-containing species $\{Cd[S_2P(OR)4\text{-}MeOPh]_2(bpy)\}_n$ for R = Me (**75**) [80] and Et (**76**) [81] are linear polymers, each with the *trans*-N_2S_4 octahedral cadmium atom located on a centre of inversion and bpy situated about a centre. In the same way, the three structures of general formula $\{Cd[S_2P(OMe)4\text{-}MeOPh]_2(N\cap N)\}_n$ for N∩N = bpe (**77**) [82], beph (**78**) [83] and dpp (**79**) [84] are very similar, all lacking symmetry, adopting zig-zag polymers and each with *cis*-N_2S_4 octahedral cadmium. The sole example of a dithiophosphinate, namely $\{Cd[S_2P(OiBu)_2]_2(bpy)\}_n$ (**80**) [85], is distinct from the aforementioned structures in that the CdNNCd axis lies on a two-fold axis of symmetry implying the coordination polymer is linear; the cadmium atom is octahedrally coordinated within a *trans*-N_2S_4 donor set.

3.6. Cadmium Dithiocarbamate Structures

As for the zinc dithiocarbamates, this section is divided into a discussion of structures incapable of hydrogen bonding and those that are capable of hydrogen bonding. In the latter category, a number of unprecedented motifs are apparent.

3.6.1. Cadmium Dithiocarbamate Structures Not Capable of Forming Hydrogen Bonds

There are only four structures in this category with four different bipyridyl-type ligands. The common feature of $\{Cd[S_2CN(CH_2Ph)_2]_2(bpy)\}_n$ (**81**) [86], with the CdNNCd axis lying on a 2-fold axis of symmetry, $[Cd(S_2CNEt_2)_2(bpe)]_n$ (**82**) [87], with two half, centrosymmetric bpe molecules in the asymmetric unit along with $Cd(S_2CNEt_2)_2$, and $[Cd(S_2CNEt_2)_2(bpeh)]_n$ (**83**) [88], with two independent repeat units in the asymmetric unit, Figure 20a, is the presence of *trans*-N_2S_4 cadmium centres and linear coordination polymers. The fourth structure, $\{Cd[S_2CN(nPr)_2]_2(2\text{-pyald})\}_2$ (**84**) [83], Figure 20b, closely resembles that of $\{Cd[S_2P(OiPr)_2]_2(2\text{-pyald})\}_2$ (**72**) [78], being a centrosymmetric dimer with a *cis*-N_2S_4 donor set owing to chelating 2-pyald ligands.

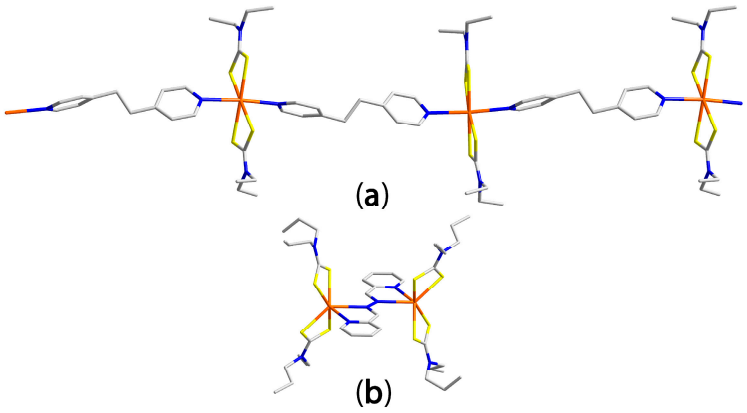

Figure 20. Supramolecular aggregation in the crystals of (**a**) $[Cd(S_2CNEt_2)_2(bpeh)]_n$ (**83**); and (**b**) $\{Cd[S_2CN(nPr)_2]_2(2\text{-pyald})\}_2$ (**84**).

3.6.2. Cadmium Dithiocarbamate Structures Capable of Forming Hydrogen Bonds

The final four structures to be described in this bibliographic review are zero-dimensional and are perhaps not of great interest in terms of the generation of coordination polymers. However, the isolation of these species raises questions relating to the relative importance of coordinate-bond formation versus hydrogen bonding interactions and, therefore, these are of fundamental interest. The molecular structures of $\{Cd[S_2CN(iPr)CH_2CH_2OH]_2(bpy)\}_2$ (**85**) [69], co-crystallised with half a bpy molecule, $\{Cd[S_2CN(iPr)CH_2CH_2OH]_2\}_2(bpe)_3$ (**86**) [90], $\{Cd[S_2CN(nPr)CH_2CH_2OH]_2\}(4\text{-pyald})_2$ (**87**) [91] and $\{Cd[S_2CN(iPr)CH_2CH_2OH]_2\}_2(3\text{-pyald})_2$ (**88**) [92] are illustrated in Figure 21a–d. In **85**, which features

a monodentate bpy ligand, the cadmium atom is five-coordinate within a NS_4 donor set that defines a geometry approaching trigonal-bipyramidal ($\tau = 0.67$) with the less tightly bound sulphur atoms defining the axial positions. A distorted *cis*-N_2S_4 donor set is found in centrosymmetric and binuclear **86** which features a bridging bpe ligand and two terminally bound bpe molecules. An octahedral geometry is also found in **87** but, based on a *trans*-N_2S_4 donor set as the cadmium centre, located on a centre on inversion, is coordinated by two monodentate 4-pyald molecules. Finally, and quite remarkably, the structure of centrosymmetric **88**, features octahedral cadmium centres within NS_5 donor sets as the 3-pyald molecules are coordinating in the monodentate mode. In all of the previous 87 structures described in this review, the original parent structure, which is often aggregated [25], has been disrupted by the addition of base. In **88**, the thermodynamically favoured dimeric structure, as opposed to the initially formed one-dimensional coordination polymer [93,94], is retained but, with the addition of base in the form of 3-pyald to increase the normally observed S_5 donor set to NS_5. These four structures, again, point to the unpredictability of this chemistry and substantiate the need of systematic studies. It is probably of no coincidence that the aforementioned four structures each feature hydrogen bonding capability in the dithiocarbamate ligands.

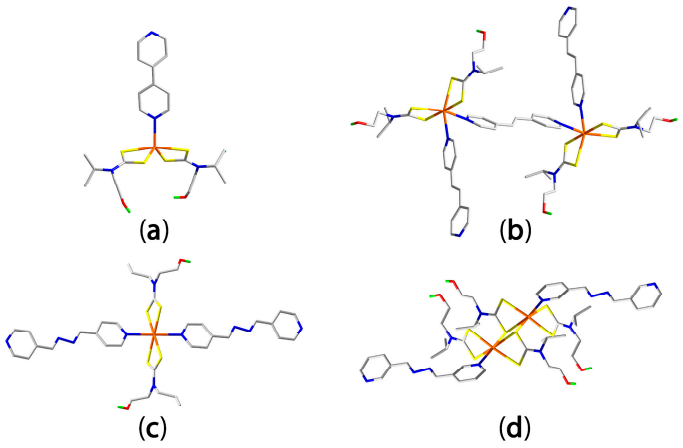

Figure 21. Aggregation in the crystals of (**a**) {$Cd[S_2CN(iPr)CH_2CH_2OH]_2(bpy)$}$_2$ (**85**); (**b**) {$Cd[S_2CN(iPr)CH_2CH_2OH]_2$}$_2$$(bpe)_3$ (**86**); (**c**) {$Cd[S_2CN(nPr)CH_2CH_2OH]_2$}$(4\text{-pyald})_2$ (**87**); and (**d**) {$Cd[S_2CN(iPr)CH_2CH_2OH]_2$}$_2$$(3\text{-pyald})_2$ (**88**).

To date, not much mention of the synthesis conditions has been made. Here, it is pertinent to note that the stoichiometry of the reactants in these reactions with functionalised dithiocarbamate ligands does not necessarily determine the synthetic outcome. For example, crystals of **86** can be isolated from solutions containing 2:1, 1:1 and 1:2 ratios of "$Cd[S_2N(iPr)CH_2CH_2OH]_2$" and bpe [90].

The structure of **85** is isostructural with the zinc analogue, **51**, and therefore the description of the molecular packing is identical to that described above, see Figure 12a. In the crystal of **86**, supramolecular layers are formed mediated by hydroxyl-O–H $\cdots$ O(hydroxyl) and hydroxyl-O–H $\cdots$ N(bpe) hydrogen bonding; that is, with the nitrogen acceptors derived from the monodentate bpe ligands, shown in Figure 22a. Layers interpenetrate to yield a three-dimensional structure, as shown in Figure 22b.

In the crystal of **87**, only hydroxyl-O–H $\cdots$ N(4-pyald) hydrogen bonds are formed and these lead to 40-membered [$CdSCNC_2OH \cdots NC_4N_2C_4N]_2$ synthons and supramolecular ladders as shown in Figure 23a. In the crystal of **88**, supramolecular layers sustained by hydroxyl-O–H $\cdots$ O(hydroxyl) and water-O–H $\cdots$ O(hydroxyl) hydrogen bonding are connected into a three-dimensional architecture via water-O–H $\cdots$ N(pyridyl) hydrogen bonding, as in Figure 23b.

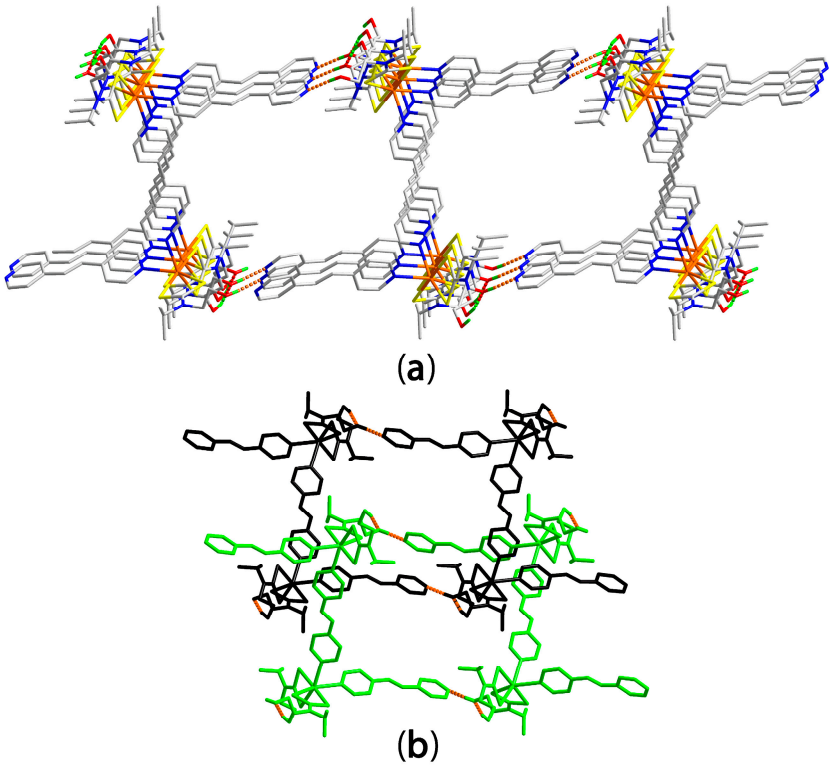

Figure 22. Supramolecular aggregation in the crystals of $\{Cd[S_2CN(iPr)CH_2CH_2OH]_2\}_2(bpe)_3$ (**86**) (**a**) layers sustained by hydroxyl-O–H ··· O(hydroxyl) and hydroxyl-O–H ··· N(bpe) hydrogen bonding; and (**b**) two-fold interpenetration of two supramolecular layers.

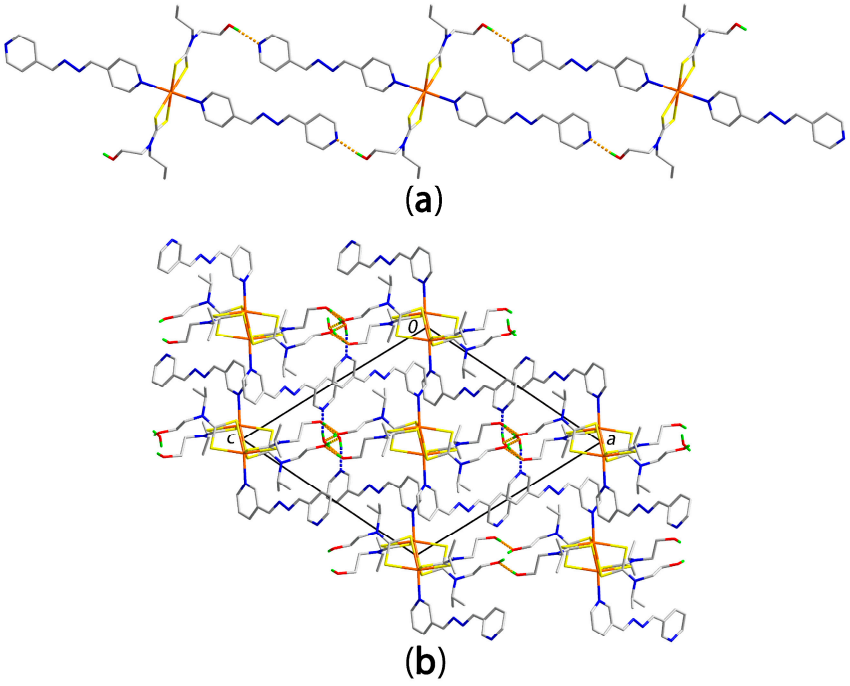

Figure 23. Supramolecular aggregation in the crystals of (**a**) $\{Cd[S_2CN(nPr)CH_2CH_2OH]_2\}(4\text{-pyald})_2$ (**87**); and (**b**) $\{Cd[S_2CN(iPr)CH_2CH_2OH]_2\}_2(3\text{-pyald})_2$ (**88**).

4. Overview and Conclusions

The foregoing overview of the structural chemistry of zinc and cadmium 1,1-dithiolates with potentially bridging bipyridyl-type ligands reveals a very real dependence upon aggregation patterns on the nature of the 1,1-dithiolate ligand as well as upon the metal centre. The maximum dimension for any coordination polymer in the structures is one, and for zinc, polymers are only formed for xanthates and dithiophosphates. For zinc dithiocarbamates, only zero-dimensional aggregates are formed; an observation which is readily rationalised in terms of the relatively greater coordination potential of the dithiocarbamate ligand compared with the other 1,1-dithiolates. This greater chelating ability arises owing to the relative importance of the resonance form where there are two formal negative charges on the sulphur atoms, Figure 24. The situation changes for cadmium where one-dimensional coordination polymers are found for all 1,1-dithiolate ligands, an observation correlating with the larger size of cadmium versus zinc.

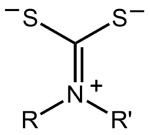

Figure 24. Chemical diagram of a significant resonance structure for the dithiocarbamate ligand. R, R′ = alkyl, aryl.

A wide array of coordination geometries are observed across the series, often arising from flexible coordination modes of xanthate and dithiophosphate ligands which range from monodentate to chelating and sometimes involve the alkoxy-O atoms in coordination. The steric role of 1,1-dithiolate-bound R groups was shown to be instrumental in controlling aggregation patterns in that larger groups, such as cyclohexyl, preclude the close approach of entities and thereby, exert an influence both over aggregation and polymer topology. A fascinating observation is made for dithiocarbamate ligands functionalised with hydrogen bonding potential, in that an apparent competition between the formation of M←N(pyridyl) coordinate-bonds and hydroxyl-O–H $\cdots$ N(pyridyl) hydrogen bonds exists leading to monodentate binding modes for the bipyridyl-type ligands. Such a competition might indicate the energy of stabilisation of these bonding modes are similar. Certainly, the unexpected structures demand further systematic studies as more insight will be gained into the fundamental coordination chemistry of metal 1,1-dithiolates.

Acknowledgments: Sunway University is gratefully acknowledged for continuing support for chemical crystallography studies.

Conflicts of Interest: The author declares no conflict of interest.

References

1. Moghadam, P.Z.; Li, A.; Wiggin, S.B.; Tao, A.; Maloney, A.G.P.; Wood, P.A.; Ward, S.C.; Fairen-Jimenez, D. Development of a Cambridge Structural Database subset: A collection of metal-organic frameworks for past, present, and future. *Chem. Mater.* **2017**, *29*, 2618–2625. [CrossRef]
2. Groom, C.R.; Bruno, I.J.; Lightfoot, M.P.; Ward, S.C. The Cambridge Structural Database. *Acta Crystallogr. B Struct. Sci. Cryst. Eng. Mater.* **2016**, *72*, 171–179. [CrossRef] [PubMed]
3. Wang, L.; Han, Y.Z.; Feng, X.; Zhou, J.W.; Qi, P.F.; Wang, B. Metal-organic frameworks for energy storage: Batteries and supercapacitors. *Coord. Chem. Rev.* **2016**, *307*, 361–381. [CrossRef]
4. Kumar, P.; Kim, K.-H.; Kwon, E.E.; Szulejko, J.E. Metal-organic frameworks for the control and management of air quality: Advances and future direction. *J. Mater. Chem. A* **2016**, *4*, 345–361. [CrossRef]
5. Noh, T.H.; Jung, O.S. Recent advances in various metal-organic channels for photochemistry beyond confined spaces. *Acc. Chem. Res.* **2016**, *49*, 1835–1843. [CrossRef] [PubMed]

6. Rogge, S.M.J.; Bavykina, A.; Hajek, J.; Garcia, H.; Olivos-Suarez, A.I.; Sepulveda-Escribano, A.; Vimont, A.; Clet, G.; Bazin, P.; Kapteijn, F. Metal-organic and covalent organic frameworks as single-site catalysts. *Chem. Soc. Rev.* **2017**, *46*, 3134–3184. [CrossRef] [PubMed]
7. D'Vries, R.F.; Iglesias, M.; Snejko, N.; Gutiérrez-Puebla, E.; Monge, M.A. Lanthanide metal-organic frameworks: Searching for efficient solvent-free catalysts. *Inorg. Chem.* **2012**, *51*, 11349–11355. [CrossRef] [PubMed]
8. He, C.; Liu, D.; Lin, W. Nanomedicine applications of hybrid nanomaterials built from metal-ligand coordination bonds: Nanoscale metal-organic frameworks and nanoscale coordination polymers. *Chem. Rev.* **2015**, *115*, 11079–11108. [CrossRef] [PubMed]
9. Johnstone, T.C.; Suntharalingam, K.; Lippard, S.J. The next generation of platinum drugs: Targeted Pt(II) agents, nanoparticle delivery, and Pt(IV) prodrugs. *Chem. Rev.* **2016**, *116*, 3436–3486. [CrossRef] [PubMed]
10. Wyszogrodzka, G.; Marszałek, B.; Gil, B.; Dorożyński, P. Metal-organic frameworks: Mechanisms of antibacterial action and potential applications. *Drug Discov. Today* **2016**, *21*, 1009–1018. [CrossRef] [PubMed]
11. Wang, H.-S. Metal-organic frameworks for biosensing and bioimaging applications. *Coord. Chem. Rev.* **2017**, *349*, 139–155. [CrossRef]
12. Anderson, S.L.; Stylianou, K.C. Biologically derived metal organic frameworks. *Coord. Chem. Rev.* **2017**, *349*, 102–128. [CrossRef]
13. Lian, X.; Fang, Y.; Joseph, E.; Wang, Q.; Li, J.L.; Banerjee, S.; Lollar, C.; Wang, X.; Zhou, H.-C. Enzyme-MOF (metal-organic framework) composites. *Chem. Soc. Rev.* **2017**, *46*, 3386–3401. [CrossRef] [PubMed]
14. Inokuma, Y.; Arai, T.; Fujita, M. Networked molecular cages as crystalline sponges for fullerenes and other guests. *Nat. Chem.* **2010**, *2*, 780–783. [CrossRef] [PubMed]
15. Hoshino, M.; Khutia, A.; Xing, H.Z.; Inokuma, Y.; Fujita, M. The crystalline sponge method updated. *IUCrJ* **2016**, *3*, 139–151. [CrossRef] [PubMed]
16. Eddaoudi, M.; Moler, D.B.; Li, H.; Chen, B.; Reineke, T.M.; O'Keeffe, M.; Yaghi, O.M. Modular chemistry: Secondary building units as a basis for the design of highly porous and robust metal-organic carboxylate frameworks. *Acc. Chem. Res.* **2001**, *34*, 319–330. [CrossRef] [PubMed]
17. Furukawa, H.; Cordova, K.E.; O'Keeffe, M.; Yaghi, O.M. The chemistry and applications of metal-organic frameworks. *Science* **2013**, *341*, 6149. [CrossRef] [PubMed]
18. Moulton, B.; Zaworotko, M.J. From molecules to crystal engineering: Supramolecular isomerism and polymorphism in network solids. *Chem. Rev.* **2001**, *101*, 1629–1658. [CrossRef] [PubMed]
19. Perry, J.J.; Perman, J.A.; Zaworotko, M.J. Design and synthesis of metal-organic frameworks using metal-organic polyhedra as supermolecular building blocks. *Chem. Soc. Rev.* **2009**, *38*, 1400–1417. [CrossRef] [PubMed]
20. Tiekink, E.R.T.; Haiduc, I. Stereochemical aspects of metal xanthate complexes: Molecular structures and supramolecular self-assembly. *Prog. Inorg. Chem.* **2005**, *54*, 127–319. [CrossRef]
21. Haiduc, I.; Sowerby, D.B. Stereochemical aspects of phosphor-1,1-dithiolato metal complexes: Coordination patterns, molecular structures and supramolecular associations in dithiophosphinates and related compounds. *Polyhedron* **1996**, *15*, 2469–2521. [CrossRef]
22. Van Zyl, W.E.; Woollins, J.D. The coordination chemistry of dithiophosphonates: An emerging and versatile ligand class. *Coord. Chem. Rev.* **2013**, *257*, 718–731. [CrossRef]
23. Heard, P.J. Main Group Dithiocarbamate Complexes. *Prog. Inorg. Chem.* **2005**, *53*, 1–69. [CrossRef]
24. Hogarth, G. Transition Metal Dithiocarbamates: 1978–2003. *Prog. Inorg. Chem.* **2005**, *53*, 71–561. [CrossRef]
25. Tiekink, E.R.T. Molecular architecture and supramolecular association in the zinc-triad 1,1-dithiolates. Steric control as a design element in crystal engineering? *CrystEngComm* **2003**, *5*, 101–113. [CrossRef]
26. Spek, A.L. Structure validation in chemical crystallography. *Acta Crystallogr. D Biol. Crystallogr.* **2009**, *65*, 148–155. [CrossRef] [PubMed]
27. *DIAMOND*, version 2.1b; K. Brandenburg & M. Berndt GbR: Bonn, Germany, 2006.
28. Ara, I.; El Bahij, F.; Lachkar, M. Synthesis, characterization and X-ray crystal structures of new ethylxanthato complexes of zinc(II) with N-donor ligands. *Synth. React. Inorg. Met.-Org. Nano-Met. Chem.* **2006**, *36*, 399–406. [CrossRef]
29. Klevtsova, R.F.; Leonova, T.G.; Glinskaya, L.A.; Larionov, S.V. Synthesis of heteroligand complexes of zinc(II) alkylxanthates with 4,4′-bipyridine. The crystal and molecular structure of the Zn_2(4,4′-Bipy)(i-$C_3H_7OCS_2)_4$·CH_2Cl_2 solvate. *Russ. J. Coord. Chem.* **2000**, *26*, 172–177.

30. Larionov, S.V.; Glinskaya, L.A.; Leonova, T.G.; Klevtsova, R.F. Polymeric structure of the complex $[Zn(4,4'\text{-Bipy})(i\text{-}BuOCS_2)_2]_n$ with monodentate isobutylxanthate ligands. *Russ. J. Coord. Chem.* **1998**, *24*, 851–856.
31. Kang, J.-G.; Shin, J.-S.; Cho, D.-H.; Jeong, Y.-K.; Park, C.; Soh, S.F.; Lai, C.S.; Tiekink, E.R.T. Steric control over supramolecular polymer formation in trans-1,2-bis(4-pyridyl)ethylene adducts of zinc xanthates: Implications for luminescence. *Cryst. Growth Des.* **2010**, *10*, 1247–1256. [CrossRef]
32. Chen, D.; Lai, C.S.; Tiekink, E.R.T. Supramolecular aggregation in diimine adducts of zinc(II) dithiophosphates: Controlling the formation of monomeric, dimeric, polymeric (zig-zag and helical), and 2-D motifs. *CrystEngComm* **2006**, *8*, 51–58. [CrossRef]
33. Zhu, D.-L.; Yu, Y.-P.; Guo, G.-C.; Zhuang, H.-H.; Huang, J.-S.; Liu, Q.; Xu, Z.; You, X.-Z. *catena*-Poly[bis(*O*,*O*′-diethyldithiophosphato-*S*)zinc(II)-μ-4,4′-bipyridyl-*N*:*N*′]. *Acta Crystallogr. C Struct. Chem.* **1996**, *52*, 1963–1966. [CrossRef]
34. Glinskaya, L.A.; Shchukin, V.G.; Klevtsova, R.F.; Mazhara, A.N.; Larionov, S.V. Synthesis and polymer structure of $[Zn(4,4'\text{-bipy})\{(i\text{-}PrO)_2PS_2\}_2]_n$ and thermal properties of $ZnL\{(i\text{-}PrO)_2PS_2\}_2$ (L = phen, 2,2′-bipy, 4,4′-bipy). *J. Struct. Chem.* **2000**, *41*, 632–639. [CrossRef]
35. Lai, C.S.; Liu, S.; Tiekink, E.R.T. Steric control over polymer formation and topology in adducts of zinc dithiophosphates formed with bridging bipyridine ligands. *CrystEngComm* **2004**, *6*, 221–226. [CrossRef]
36. Welte, W.B.; Tiekink, E.R.T. *catena*-Poly[[bis(*O*,*O*′-diisopropyl dithiophosphato-κ^2S,S')zinc(II)]-μ-1,2-di-4-pyridylethylene-κ^2N:*N*′]. *Acta Crystallogr. E Crystallogr. Commun.* **2007**, *63*, m790–m792. [CrossRef]
37. Welte, W.B.; Tiekink, E.R.T. *catena*-Poly[[bis(*O*,*O*′-diisobutyl dithiophosphato-κ^2S,S')zinc(II)]-μ-1,2-di-4-pyridylethylene-κ^2N:*N*′]. *Acta Crystallogr. E Crystallogr. Commun.* **2006**, *62*, m2070–m2072. [CrossRef]
38. Tiekink, E.R.T.; Wardell, J.L.; Welte, W.B. *catena*-Poly[[bis(*O*,*O*′-diethyl dithiophosphato-κ^2S,S')zinc(II)]-μ-1,2-di-4-pyridylethane-κ^2N:*N*′]. *Acta Crystallogr. E Crystallogr. Commun.* **2007**, *63*, m818–m820. [CrossRef]
39. Lai, C.S.; Liu, S.; Tiekink, E.R.T. *catena*-Poly[[bis(*O*,*O*′-diisobutyldithiophosphato-κ^2S,S')zinc(II)]-μ-1,2-bis(4-pyridyl)ethane-κ^2N:*N*′]. *Acta Crystallogr. E Crystallogr. Commun.* **2004**, *60*, m1005–m1007. [CrossRef]
40. Chen, D.; Lai, C.S.; Tiekink, E.R.T. *catena*-Poly[[bis(*O*,*O*′-dicyclohexyldithiophosphato-κ^2S,S')zinc(II)]-μ-1,2-bis(4-pyridylmethylene)hydrazine-κ^2N:*N*′]. *Acta Crystallogr. E Crystallogr. Commun.* **2005**, *61*, m2052–m2054. [CrossRef]
41. Avila, V.; Tiekink, E.R.T. *catena*-Poly[[bis(*O*,*O*′-diisopropyl dithiophosphato-κ^2S,S')zinc(II)]-μ-1,2-bis (3-pyridylmethylene)hydrazine-κ^2N:*N*′]. *Acta Crystallogr. E Crystallogr. Commun.* **2006**, *62*, m3530–m3531. [CrossRef]
42. Devillanova, F.; Aragoni, C.; Arca, M.; Huth, S.L.; Hursthouse, M.B. CAGLIARI 154a - $C_{28}H_{32}N_2O_4P_2S_4Zn_1$. *Pers. Commun. Camb. Str. Database* **2008**. [CrossRef]
43. Shchukin, V.G.; Glinskaya, L.A.; Klevtsova, R.F.; Larionov, S.V. Synthesis, structure, and thermal properties of heteroligand coordination compounds $ZnL\{(i\text{-}C_4H_9)_2PS_2\}_2$ (L = Phen, 2,2′-Bipy, or 4,4′-Bipy). Polymeric structure of $[Zn(4,4'\text{-Bipy})\{(i\text{-}C_4H_9)_2PS_2\}_2]_n$. *Russ. J. Coord. Chem.* **2000**, *26*, 331–337.
44. Klevtsova, R.F.; Glinskaya, L.A.; Berus, E.I.; Larionov, S.V. Monodentate and bridging bidentate functions of 4,4′-bipyridine in the crystal structures of $[Zn(4,4'\text{-Bipy})\{(n\text{-}C_3H_7)_2NCS_2\}_2]$ and $[Zn_2(4,4'\text{-Bipy})\{(n\text{-}C_3H_7)_2NCS_2\}_4]$. *J. Str. Chem.* **2001**, *42*, 639–647. [CrossRef]
45. Zha, M.-Q.; Li, X.; Bing, Y.; Lu, Y. μ-4,4′-Bipyridine-κ^2N:*N*′)bis[bis(*N*,*N*-dimethyldithiocarbamato-κ^2S,S')zinc (II)]. *Acta Crystallogr. E Crystallogr. Commun.* **2010**, *66*, m1465. [CrossRef]
46. Zemskova, S.M.; Glinskaya, L.A.; Durasov, V.B.; Klevtsova, R.F.; Larionov, S.V. Mixed-ligand complexes of zinc(II) and cadmium(II) diethyldithiocarbamates with 2,2′-bipyridyl and 4,4′-bipyridyl-synthesis, structure, and thermal-properties. *J. Struct. Chem.* **1993**, *34*, 794–802. [CrossRef]
47. Lai, C.S.; Tiekink, E.R.T. (4,4′-Bipyridine)bis[bis(*N*,*N*-diethyldithiocarbamato)zinc(II)]. *Appl. Organomet. Chem.* **2003**, *17*, 253–254. [CrossRef]
48. Larionov, S.V.; Klevtsova, R.F.; Shchukin, V.G.; Glinskaya, L.A.; Zemskova, S.M. Heteroligand complexes of Zn(II) diisopropyl dithiocarbamate with 1,10-phenanthroline and 4,4′-bipyridlne. Crystal and molecular structures of clathrate compound $Zn(4,4'\text{-Bipy})((i\text{-}C_3H_7)_2NCS_2)_4{\cdot}2C_6H_5CH_3$. *Russ. J. Coord. Chem.* **1999**, *25*, 694–700.

49. Zemskova, S.M.; Glinskaya, L.A.; Klevtsova, R.F.; Durasov, V.B.; Gromilov, S.A.; Larionov, S.V. Volatile mixed-ligand complexes of bis(diisobutyldithiocarbamato)zinc with 1,10-phenanthroline, 2,2′-bipyridyl, and 4,4′-bipyridyl. Crystal and molecular structure of the binuclear complex $[Zn_2(C_{10}H_8N_2)\{(i\text{-}C_4H_9)2NCS_2\}_4]$. *J. Struct. Chem.* **1996**, *37*, 941–947. [CrossRef]
50. Yin, X.; Zhang, W.; Fan, J.; Wei, F.X.; Lai, C.S.; Tiekink, E.R.T. Bis[bis(*N*,*N*-dibenzyldithiocarbamato)zinc(II)] (4,4′-bipyridine). *Appl. Organomet. Chem.* **2003**, *17*, 889–890. [CrossRef]
51. Chen, X.-F.; Liu, S.-H.; Zhu, X.-H.; Vittal, J.J.; Tan, G.-K.; You, X.-Z. μ-(4,4′-Bipyridine)-*N*:*N*′-bis [bis-(pyrrolidinedithiocarboxylato-*S*,*S*′)zinc(II)]. *Acta Crystallogr. C Struct. Chem.* **2000**, *56*, 42–43. [CrossRef]
52. Liu, S.-H.; Chen, X.-F.; Zhu, X.-H.; Duan, C.-Y.; You, X.-Z. Crystal structure and thermal analysis of a 4,4′-bipy-bridged binuclear zinc(II) complex, $2[R_2NCS_2]_2{\cdot}Zn(4,4'\text{-bipy})$ (R = piperidyl). *J. Coord. Chem.* **2001**, *53*, 223–231. [CrossRef]
53. Poplaukhin, P.; Tiekink, E.R.T. (μ-1,2-Di-4-pyridylethylene-κ^2N:*N*′)bis[bis(*N*,*N*-dimethyldithiocarbamato-κ^2S,*S*′)zinc(II)]. *Acta Crystallogr. E Crystallogr. Commun.* **2009**, *65*, m1474. [CrossRef]
54. Arman, H.D.; Poplaukhin, P.; Tiekink, E.R.T. (μ-trans-1,2-Di-4-pyridylethylene-κ^2N:*N*′)bis[bis(*N*,*N*-diethyldithiocarbamato-κ^2S,*S*′)zinc(II)] chloroform solvate. *Acta Crystallogr. E Crystallogr. Commun.* **2009**, *65*, m1472–m1473. [CrossRef]
55. Arman, H.D.; Poplaukhin, P.; Tiekink, E.R.T. (μ-trans-1,2-Di-4-pyridylethylene-κ^2N:*N*′)bis[bis(*N*,*N*-diisopropyldithiocarbamato-κ^2S,*S*′)zinc(II)]. *Acta Crystallogr. E Crystallogr. Commun.* **2009**, *65*, m1475. [CrossRef]
56. Lai, C.S.; Tiekink, E.R.T. Bis[bis(*N*,*N*-diethyldithiocarbamato)zinc(II)] (trans-1,2-bis(4-pyridyl)ethylene) trans-1,2-bis(4-pyridyl)ethylene lattice adduct. *Appl. Organomet. Chem.* **2003**, *17*, 251–252. [CrossRef]
57. Avila, V.; Tiekink, E.R.T. μ-1,2-Di-4-pyridylethane-κ^2N:*N*′-bis[bis(*N*,*N*-diisopropyldithiocarbamato-κ^2S,*S*′) zinc(II)]. *Acta Crystallogr. E Crystallogr. Commun.* **2008**, *64*, m680. [CrossRef]
58. Arman, H.D.; Poplaukhin, P.; Tiekink, E.R.T. Crystal structure of (μ_2-*N*,*N*′-bis((pyridin-4-yl)methyl) ethanediamide-κ^2N:*N*′)-tetrakis(diethylcarbamodithioato-κ^2S,*S*′)dizinc(II), $C_{34}H_{54}N_8O_2S_8Zn_2$. *Z. Krist. New Cryst. Struct.* **2017**, in press. [CrossRef]
59. Arman, H.D.; Poplaukhin, P.; Tiekink, E.R.T. Crystal structures of {μ_2-*N*,*N*′-bis[(pyridin-3-yl)-methyl] ethanediamide}tetrakis(dimethylcarbamodithioato)dizinc(II) dimethylformamide disolvate and {{μ_2-*N*,*N*′-bis[(pyridin-3-yl)methyl]ethanediamide}tetrakis(di-*n*-propylcarbamodithioato)-dizinc(II). *Acta Crystallogr. E Crystallogr. Commun.* **2017**, *73*, 1501–1507. [CrossRef] [PubMed]
60. Jotani, M.M.; Poplaukhin, P.; Arman, H.D.; Tiekink, E.R.T. Supramolecular association in (μ_2-pyrazine)-tetrakis(*N*,*N*-bis(2-hydroxyethyl)dithiocarbamato)dizinc(II) and its di-dioxane solvate. *Z. Krist.* **2017**, *232*, 287–298. [CrossRef]
61. Benson, R.E.; Ellis, C.A.; Lewis, C.E.; Tiekink, E.R.T. 3D-, 2D- and 1D-supramolecular structures of $\{Zn[S_2CN(CH_2CH_2OH)R]_2\}_2$ and their $\{Zn[S_2CN(CH_2CH_2OH)R]_2\}_2$(4,4′-bipyridine) adducts for R = CH_2CH_2OH, Me or Et: Polymorphism and pseudo-polymorphism. *CrystEngComm* **2007**, *9*, 930–940. [CrossRef]
62. Tan, Y.S.; Tiekink, E.R.T. Crystal structure of (4,4′-bipyridyl-κ*N*)bis[*N*-(2-hydroxyethyl)-*N*-isopropyldithiocarbamato-κ^2S,*S*′]-zinc(II)–4,4′-bipyridyl (2/1) and its isostructural cadmium(II) analogue. *Acta Crystallogr. E Crystallogr. Commun.* **2017**, *73*, 1642–1646. [CrossRef] [PubMed]
63. Broker, G.A.; Jotani, M.M.; Tiekink, E.R.T. Bis[*N*-2-hydroxyethyl,*N*-methyldithiocarbamato-κ^2S,*S*)′-4-{[(pyridin-4-ylmethylidene)hydrazinylidene}methyl]pyridine-κN^1)zinc(II): Crystal structure and Hirshfeld surface analysis. *Acta Crystallogr. E Crystallogr. Commun.* **2017**, *73*, 1458–1564. [CrossRef] [PubMed]
64. Poplaukhin, P.; Tiekink, E.R.T. Interwoven coordination polymers sustained by tautomeric forms of the bridging ligand. *CrystEngComm* **2010**, *12*, 1302–1306. [CrossRef]
65. Poplaukhin, P.; Arman, H.D.; Tiekink, E.R.T. Supramolecular isomerism in coordination polymers sustained by hydrogen bonding: Bis[$Zn(S_2CN(Me)CH_2CH_2OH)_2$](*N*,*N*′-bis(pyridin-3-ylmethyl)thioxalamide). *Z. Krist.* **2012**, *227*, 363–368. [CrossRef]
66. Arman, H.D.; Poplaukhin, P.; Tiekink, E.R.T. Bis[*N*-(2-hydroxyethyl)-*N*-methyldithiocarbamato-κ*S*][2,4,6-tris (pyridin-2-yl)-1,3,5-triazine-κ^3N^1,N^2,N^6]zinc dioxane sesquisolvate. *Acta Crystallogr. E Crystallogr. Commun.* **2012**, *68*, m319–m320. [CrossRef]
67. Ikeda, T.; Hagihara, H. The crystal structure of zinc ethylxanthate. *Acta Crystallogr.* **1966**, *21*, 919–927. [CrossRef]

68. Lai, C.S.; Lim, Y.X.; Yap, T.C.; Tiekink, E.R.T. Molecular paving with zinc thiolates. *CrystEngComm* **2002**, *4*, 596–600. [CrossRef]
69. Addison, A.W.; Rao, T.N.; Reedijk, J.; van Rijn, J.; Verschoor, G.C. Synthesis, structure, and spectroscopic properties of copper(II) compounds containing nitrogen-sulphur donor ligands; the crystal and molecular structure of aqua[1,7-bis(*N*-methylbenzimidazol-2′-yl)-2,6-dithiaheptane]copper(II) perchlorate. *J. Chem. Soc. Dalton Trans.* **1984**, 1349–1356. [CrossRef]
70. Tiekink, E.R.T. Aggregation patterns in the crystal structures of organometallic Group XV 1,1-dithiolates: The influence of the Lewis acidity of the central atom, metal- and ligand-bound steric bulk, and coordination potential of the 1,1-dithiolate ligands upon supramolecular architecture. *CrystEngComm* **2006**, *8*, 104–118. [CrossRef]
71. Jotani, M.M.; Zukerman-Schpector, J.; Sousa Madureira, L.; Poplaukhin, P.; Arman, H.D.; Miller, T.; Tiekink, E.R.T. Structural, Hirshfeld surface and theoretical analysis of two conformational polymorphs of *N*,*N*′-bis(pyridin-3-ylmethyl)oxalamide. *Z. Krist.* **2016**, *231*, 415–425. [CrossRef]
72. Zukerman-Schpector, J.; Sousa Madureira, L.; Poplaukhin, P.; Arman, H.D.; Miller, T.; Tiekink, E.R.T. Conformational preferences for isomeric *N*,*N*′-bis(pyridin-*n*-ylmethyl)ethanedithiodiamides, *n* = 2, 3 and 4: A combined crystallographic and DFT study. *Z. Krist.* **2015**, *230*, 531–541. [CrossRef]
73. Jamaludin, N.S.; Halim, S.N.A.; Khoo, C.-H.L.; Chen, B.-J.; See, T.-H.L.; Sim, J.-H.; Cheah, Y.-K.; Seng, H.-L.; Tiekink, E.R.T. Bis(phosphane)copper(I) and silver(I) dithiocarbamates: Crystallography and anti-microbial assay. *Z. Krist.* **2016**, *231*, 341–349. [CrossRef]
74. Abrahams, B.F.; Hoskins, B.F.; Winter, G. The structure of cadmium bis(isopropylxanthate)-4,4′-bipyridine. *Aust. J. Chem.* **1990**, *43*, 1759–1765. [CrossRef]
75. Li, T.; Li, Z.-H.; Du, S.-W. *catena*-Poly[[bis(*O*,*O*′-dimethyl dithiophosphato-κ^2S,*S*′)cadmium(II)]-μ-4,4′-bipyridine-*N*:*N*′]. *Acta Crystallogr. E Crystallogr. Commun.* **2005**, *61*, m95–m97. [CrossRef]
76. Li, T.; Li, Z.-H.; Du, S.-W. *catena*-Poly[[bis(*O*,*O*′-diethyl dithiophosphato-κ^2S,*S*′)cadmium(II)]-μ-4,4′-bipyridine-*N*:*N*′]. *Acta Crystallogr. E Crystallogr. Commun.* **2004**, *60*, m1912–m1914. [CrossRef]
77. Lai, C.S.; Tiekink, E.R.T. Engineering polymers with variable topology—Bipyridine adducts of cadmium dithiophosphates. *CrystEngComm* **2004**, *6*, 593–605. [CrossRef]
78. Lai, C.S.; Tiekink, E.R.T. Polymeric topologies in cadmium(II) dithiophosphate adducts of the isomeric *n*-pyridinealdazines, *n* = 2, 3 and 4. *Z. Krist.* **2006**, *221*, 288–293. [CrossRef]
79. Lai, C.S.; Tiekink, E.R.T. Delineating the principles controlling polymer formation and topology in zinc(II)- and cadmium(II)-dithiophosphate adducts of diimine-type ligands. *J. Mol. Struct.* **2006**, *796*, 114–118. [CrossRef]
80. Devillanova, F.; Aragoni, C.; Arca, M.; Huth, S.L.; Hursthouse, M.B. CAGLIARI 143-$C_{26}H_{28}Cd_1N_2O_4P_2S_4$. *Pers. Commun. Camb. Str. Database* **2008**. [CrossRef]
81. Devillanova, F.; Aragoni, C.; Arca, M.; Hursthouse, M.B.; Huth, S.L. CAGLIARI 161-$C_{28}H_{32}Cd_1N_2O_4P_2S_4$. *Pers. Commun. Camb. Str. Database* **2008**. [CrossRef]
82. Devillanova, F.; Aragoni, C.; Arca, M.; Huth, S.L.; Hursthouse, M.B. CAGLIARI 145-$C_{28}H_{30}Cd_1N_2O_4P_2S_4$. *Pers. Commun. Camb. Str. Database* **2008**. [CrossRef]
83. Devillanova, F.; Aragoni, C.; Arca, M.; Huth, S.L.; Hursthouse, M.B. CAGLIARI 144a-$C_{28}H_{32}Cd_1N_2O_4P_2S_4$. *Pers. Commun. Camb. Str. Database* **2008**. [CrossRef]
84. Devillanova, F.; Aragoni, C.; Arca, M.; Hursthouse, M.B.; Huth, S.L. CAGLIARI 142-$C_{29}H_{34}Cd_1N_2O_4P_2S_4$. *Pers. Commun. Camb. Str. Database* **2008**. [CrossRef]
85. Larionov, S.V.; Shchukin, V.G.; Glinskaya, L.A.; Klevtsova, R.F.; Mazhara, A.P. Mixed-ligand coordination compounds $CdL\{(i\text{-}C_4H_9)_2PS_2\}_2$ (L = phen, 2,2′-Bipy, and 4,4′-Bipy): Synthesis, structure, and thermal properties. Polymeric structure of $[Cd(4,4'\text{-Bipy})\{(i\text{-}C_4H_9)_2PS_2\}_2]_n$. *Russ. J. Coord. Chem.* **2001**, *27*, 463–468. [CrossRef]
86. Fan, J.; Wei, F.-X.; Zhang, W.-G.; Yin, X.; Lai, C.S.; Tiekink, E.R.T. Small ligands-induced synthesis of cadmium complexes with *N*,*N*-dibenzyl dithiocarbamate and their crystal structures. *Acta Chim. Sin.* **2007**, *65*, 2014–2018.
87. Chai, J.; Lai, C.S.; Yan, J.; Tiekink, E.R.T. Polymeric [bis(*N*,*N*-diethyldithiocarbamato) (*trans*-1,2-bis (4-pyridyl)ethylene)cadmium(II)]. *Appl. Organomet. Chem.* **2003**, *17*, 249–250. [CrossRef]

88. Avila, V.; Benson, R.E.; Broker, G.A.; Daniels, L.M.; Tiekink, E.R.T. *catena*-Poly[[bis(*N*,*N*-diethyldithiocarbamato-κ^2S,S')cadmium(II)]-μ-trans-1,2-di-4-pyridylethane-$\kappa^2N:N'$]. *Acta Crystallogr. E Crystallogr. Commun.* **2006**, *62*, m1425–m1427. [CrossRef]
89. Poplaukhin, P.; Tiekink, E.R.T. (μ-2-Pyridinealdazine-$\kappa^4N,N':N'',N'''$)bis[bis(*N*,*N*-di-n-propyldithiocarbamato-κ^2S,S')cadmium(II)]. *Acta Crystallogr. E Crystallogr. Commun.* **2008**, *64*, m1176. [CrossRef]
90. Jotani, M.M.; Poplaukhin, P.; Arman, H.D.; Tiekink, E.R.T. [μ_2-trans-1,2-Bis(pyridin-4-yl)ethene-$\kappa^2N:N'$] bis{[1,2-bis(pyridin-4-yl)ethene-κN]bis[*N*-(2-hydroxyethyl)-*N*-isopropyldithiocarbamato-κ^2S,S']cadmium} acetonitrile tetrasolvate: Crystal structure and Hirshfeld surface analysis. *Acta Crystallogr. E Crystallogr. Commun.* **2016**, *72*, 1085–1092. [CrossRef] [PubMed]
91. Broker, G.A.; Tiekink, E.R.T. Bis[*N*-(2-hydroxyethyl)-*N*-propyldithiocarbamato-κ^2S,S']bis(4-{[(pyridin-4-ylmethylidene)hydrazinylidene]methyl}pyridine-κN^1)cadmium. *Acta Crystallogr. E Crystallogr. Commun.* **2011**, *67*, m320–m321.
92. Arman, H.D.; Poplaukhin, P.; Tiekink, E.R.T. An unprecedented binuclear cadmium dithiocarbamate adduct: Bis[μ_2-*N*-(2-hydroxyethyl)-*N*-isopropylcarbamodithioato-$\kappa^3S:S,S'$]bis{[*N*-(2-hydroxyethyl)-*N*-isopropylcarbamodithioato-κ^2S,S'](3-{(1E)-[(E)-2-(pyridin-3-ylmethylidene)hydrazin-1-ylidene]methyl}-pyridine-κN)cadmium]} dihydrate. *Acta Crystallogr. E Crystallogr. Commun.* **2016**, *72*, 1234–1238. [CrossRef] [PubMed]
93. Tan, Y.S.; Sudlow, A.L.; Molloy, K.C.; Morishima, Y.; Fujisawa, K.; Jackson, W.J.; Henderson, W.; Halim, S.N.B.A.; Ng, S.W.; Tiekink, E.R.T. Supramolecular isomerism in a cadmium bis(*N*-hydroxyethyl, *N*-isopropyldithiocarbamate) compound: Physiochemical characterization of ball (n = 2) and chain (n = ∞) forms of $\{Cd[S_2CN(iPr)CH_2CH_2OH]_2 \cdot solvent\}_n$. *Cryst. Growth Des.* **2013**, *13*, 3046–3056. [CrossRef]
94. Tan, Y.S.; Halim, S.N.A.; Tiekink, E.R.T. Exploring the crystallization landscape of cadmium bis(*N*-hydroxyethyl, *N*-isopropyl-dithiocarbamate), $Cd[S_2CN(iPr)CH_2CH_2OH]_2$. *Z. Krist.* **2016**, *231*, 113–126. [CrossRef]